tion, motility, and morphology in adult mice. Our data suggest that UCHL1-dependent apoptosis is essential for normal spermatogenesis.

MATERIALS AND METHODS

Animals

We used male *gad* (CBA/RFM) mice [21] at 7, 14, 21, 28, and 35 days and 10 wk of age. The *gad* mouse is an autosomal-recessive mutant that was produced by crossing CBA and RFM mice. The *gad* line was maintained by intercrossing for more than 20 generations. This strain was maintained at our institute. Animal care and handling were in accordance with institutional regulations and were approved by the Animal Investigation Committee of the National Institute of Neuroscience, National Center of Neurology and Psychiatry.

Histological and Immunohistochemical Assessment of Testes

Testes were embedded in paraffin wax after fixation in 4% paraformaldehyde, sectioned at 4-μm thickness, and stained with hematoxylin for counting [13]. Light microscopy was used for routine observations. For immunohistochemical staining, the sections were incubated with 10% goat serum for 1 h at room temperature followed by incubation overnight at 4°C with a rabbit polyclonal antibody against UCHL1 (1:1000 dilution; peptide antibody) [20] in PBS containing 1% BSA. Sections were then incubated for 1 h with biotin-conjugated anti-rabbit IgG diluted 1:200 in PBS, followed by Vectorstain ABC-PO (Vector Laboratories, Burlingame, CA) for 30 min at room temperature. Sections were developed using 3,3′-diaminobenzidine and counterstained with hematoxylin.

Apoptotic cells in testicular tissues were identified by terminal deoxynucleotidyl transferase (TdT)-mediated nick end labeling (TUNEL) using the DeadEnd Fluorometric TUNEL system (Promega, Madison, WI) according to the manufacturer's instructions.

Quantitative Analysis of Testicular Cell Number

The total number of cells was determined by counting the testicular cells including Sertoli cells of seminiferous tubules. Quantitative determinations were made using four each of wild-type and *gad* mice at 7 and 14 days of age. Five sections from each mouse were processed in parallel for counterstaining with hematoxylin. Twenty circular seminiferous tubules in each section were then selected by randomly from those tubules, and 400 circular seminiferous tubules were measured using the 400× lens of a Zeiss Axioplan microscope. The total cell number was not determined by dividing cell types such as testicular germ cells and Sertoli cells because it was difficult to determine the difference of cell types [26]. There were no significant differences in nuclear size in either of the group studies. Thus, the total number of cells reflected all cell types of seminiferous tubules.

Quantitative Analysis of Apoptotic Germ Cells

Quantification was performed using four each of wild-type and *gad* mice at 7, 14, 21, 28, and 35 days of age. The total number of apoptotic cells was determined by counting the positively stained nuclei in 20 circular seminiferous tubules in each section [22]. Five sections from each mouse and a total 400 circular seminiferous tubules per each group were processed.

Germ Cell Isolation, Culture, and Viability Measurement

Germ cells from wild-type and *gad* mice were prepared using a modification of the procedure described by Kwon et al. [20]. Briefly, testes from three 2-wk-old mice were incubated twice for 30 min at 25°C in Dulbecco Modified Eagle medium (DMEM)-F12 medium containing 0.5 mg/ml collagenase IV-S (Sigma-Aldrich, St. Louis, MO) and then digested for 60 min at 25°C in DMEM-F12 medium containing 1 mg/ml trypsin (Sigma-Aldrich). The cell suspension was digested and washed several times to eliminate testicular somatic cells. The cells were then counted and cultured at 2.0×10^5 cells/ml in DMEM-F12 medium containing 10% fetal bovine serum (FBS). The cells were harvested at each day for 5 days, and viability was assessed using the Vi-Cell XR cell viability analyzer (Beckman Coulter, Fullerton, CA).

Quantitative mRNA Analysis of Uchl1 and Uchl3 Genes by Real-Time PCR

SYBR Green-based real-time quantitative reverse transcription-polymerase chain reaction (RT-PCR; PRISM 7700 Sequence detection system, ABI, Columbia, MD) was performed [20] in SYBR Green Master mix using the following primers: *Uchl1*, 5′-TTCTGTTCAACAACGTGGACG-3′ and 5′-TCACTGGAAAGGGCATTCG-3′; *Uchl3*, 5′-TGAAGGTCAGACTGAGGCACC-3′ and 5′-AATTGGAAATGGTTTCCGTCC-3′; β-actin, 5′-CGTGCGTGACATCAAAGAGAA-3′ and 5′-CAATAGTGATGACCTGGCCGT-3′ To compare *Uchl1* and *Uchl3* gene expression in the first round of spermatogenesis, the formula 2^{-ddCt} was used to calculate relative expression compared with testes of 7-day-old mice.

Western Blotting

Western blots were performed as previously reported [19, 22]. Total protein (5 μg/lane) was subjected to SDS-polyacrylamide gel electrophoresis using 15% gels (Perfect NT Gel, DRC, Japan). Proteins were electrophoretically transferred to polyvinylidene difluoride membranes (Bio-Rad, Hercules, CA) and blocked with 5% nonfat milk in TBS-T (50 mM Tris base, pH 7.5, 150 mM NaCl, 0.1% [w/v] Tween-20). The membranes were incubated individually with one or more primary antibodies to UCHL1 and UCHL3 (1:1000 dilution; peptide antibodies) [20], Bcl-xL, Bax, TRP53, and inactive caspase-3 (1:1000 dilution; all from Cell Signaling Technology, Beverly, MA). Blots were further incubated with peroxidase-conjugated goat anti-mouse IgG or goat anti-rabbit IgG (1:5000 dilution; Pierce, Rockford, IL) for 1 h at room temperature. Immunoreactions were visualized using the SuperSignal West Dura Extended Duration Substrate (Pierce) and analyzed using a ChemiImager (Alpha Innotech, San Leandro, CA).

Sperm Motility, Morphology, and Immunohistochemical Assessments

Sperm were collected from the right cauda epididymidis [27] of 10-wk-old wild-type and *gad* mice in 400 μl human tubal fluid medium containing 0.5% bovine serum albumin and then incubated at 37°C under 5% CO_2 in air for 1–2 h. Using a computer-assisted semen analysis system (TOX IVOS, Hamilton Throne Research, Beverly, MA) [28], sperm were analyzed for the following motion parameters: percentage of motile sperm (MSP), percentage of progressively motile sperm (PMP), average path velocity (VAP), straight-line velocity (VSL), curvilinear velocity (VCL), lateral head displacement (ALH), linearity (VSL/VCL × 100), and straightness (VSL/VAP × 100). All procedures were performed at 37°C. To study the spermatozoa morphology, sperm were smeared and then evaluated for defects in the head, midpiece, and principal piece and for head detachment. For immunocytochemical staining, the sections were incubated with antibodies against UCHL1 (1:1000 dilution; peptide antibody) [20] and ubiquitin (1:500 dilution; DakoCytomation, Glostrup, Denmark) overnight at 4°C in PBS containing 1% BSA.

Statistical Analysis

The mean and standard deviation were calculated for all data (presented as mean ± SD). One-way analysis of variance (ANOVA) was used for all statistical analyses.

RESULTS

Expression of UCHL1 During the First Round of Spermatogenesis

We used Western blotting to characterize the level of UCHL1 and UCHL3 expression in testes from immature wild-type and *gad* mice (Fig. 1, B and C). In agreement with previous data [20], UCHL1 expression was significantly elevated on Day 14 in testicular lysates obtained from 7-, 14-, 21-, 28-, and 35-day-old wild-type mice. The level of UCHL3 expression increased with age and did not differ between *gad* and wild-type mice (Fig. 1B), suggesting that UCHL3 expression is regulated independently of UCH-L1 during the first round of spermatogenesis [20]. We also assessed the expression pattern of *Uchl1* and *Uchl3* genes during juvenile spermatogenesis using SYBR Green-

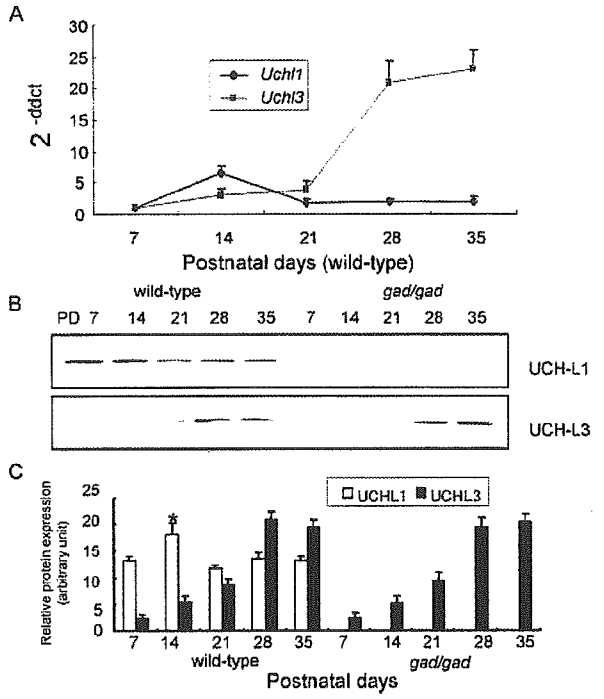

FIG. 1. Expression of UCHL1 and UCHL3during the first round of spermatogenesis. **A**) Comparison of *Uchl1* and *Uchl3* gene expression levels (2^{-ddCt}) by SYBR Green-based real-time quantitative reverse transcription-polymerase chain reaction (RT-PCR). The value for gene expression from the testes of 7-day-old mice was set to 1.0. **B**) Comparison of UCHL1 and UCHL3 expression by Western blotting of testicular lysates from wild-type or *gad* mice. Blots were reprobed for α-tubulin, which was used to normalize the protein load. Representative images from four independent experiments are shown. **C**) Quantitative analysis of changes in UCHL1 and UCHL3 levels by Western blotting. Relative protein expression (optical density) of the bands in panel **B**, normalized to α-tubulin. Each data point represents the mean ± SD (n = 4; * $P < 0.05$).

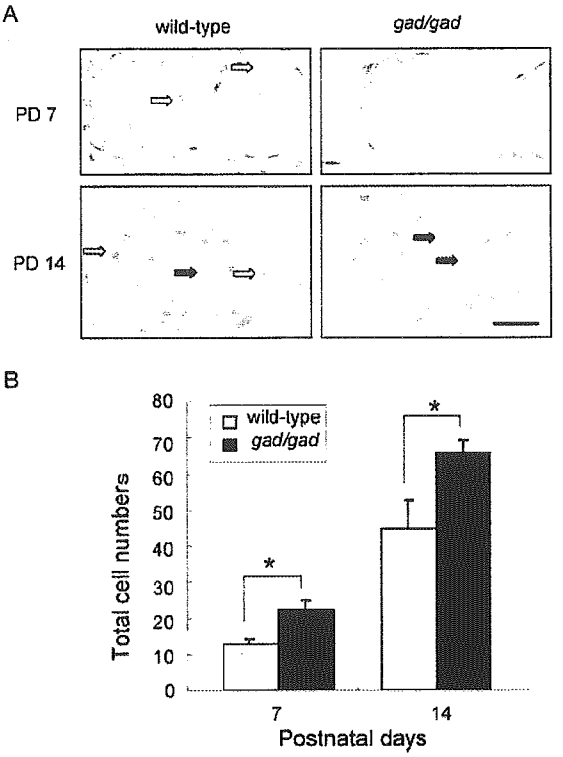

FIG. 2. **A**) Immunohistochemistry of UCHL1 and testicular morphology during the first round of spermatogenesis. UCHL1-positive germ cells in wild-type mice are indicated by open arrows. Spermatogonia and preleptotene spermatocytes (closed arrows) were more abundant and found further from the basement membrane in Postnatal Day (PD) 7 and 14 *gad* mice. Magnification ×200. Bar = 20 μm. **B**) The total number of germ cells in seminiferous tubules was significantly increased in and 7- and 14-day-old *gad* mice compared with wild-type mice (n = 4; * $P < 0.05$). Data represent mean ± SD.

based real-time quantitative RT-PCR (Fig. 1A). Despite the fact that the percentage of spermatogonia and Sertoli cells may be diluted by meiotic and postmeiotic germ cells after Day 14 [20], *Uchl1* expression was high in 14-day-old mice, in agreement with our previous findings.

Immunohistochemistry of UCHL1 and Quantitative Morphometric Assessment

Immunohistochemical analysis revealed UCHL1 expression in spermatogonia from wild-type mice but not *gad* mice (Fig. 2A). Preliminary examination of tubules from immature testes revealed an overproduction of germ cells in *gad* mice. At 7 and 14 days of age, the number of spermatogonia and preleptotene spermatocytes was significantly increased in *gad* mice compared with wild-type mice (Fig. 2A). The increase in the number of these cell types was further confirmed by quantitative analysis, which showed that the total number of testicular cells, including Sertoli cells, was significantly higher in 7- and 14-day-old *gad* mice (Fig. 2B).

TUNEL Staining of Apoptotic Germ Cells During the First Round of Spermatogenesis

To further investigate the mechanism underlying the observed differences in testicular cell numbers between wild-type and *gad* mice during the first round of spermatogenesis, we examined germ cell apoptosis in tissue sections from mice at 7, 14, 21, 28, and 35 days of age by TUNEL assay. During the first round of spermatogenesis, the total number of apoptotic cells in 20 circular seminiferous tubules decreased significantly (n = 4; $P < 0.05$) in gad mouse testes as compared with wild-type mice (Fig. 3A). Although germ cell apoptosis significantly increased at Day 14 in the testes of both wild-type and *gad* mice, *gad* mice had significantly fewer apoptotic germ cells (n = 4; $P < 0.05$) in seminiferous tubules (Fig. 3B).

Testicular Germ Cells of gad *Mice Are Resistant to Apoptosis-Inducing Conditions In Vitro*

Sertoli cells, which support germ cells, express UCHL1 [12]. To explore the viability of germ cells independently of the effect of Sertoli cells, testicular germ cells from 2-wk-old wild-type and *gad* mice were cultured in suspension for 5 days in the presence of 10% FBS. We then examined the resistance of these in vitro cell culture to apoptosis-inducing conditions. Although both wild-type and *gad* mouse cells were sensitive to apoptosis-inducing conditions, the *gad* mouse cells had comparatively greater viability (Fig. 4). Overall results clearly show that the absence of UCHL1 increase germ cell survival.

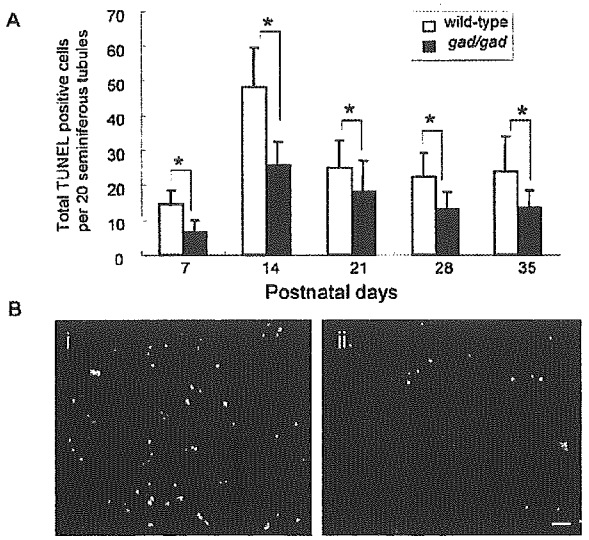

FIG. 3. A) The total TUNEL-positive germinal cells per 20 circular seminiferous tubules in wild-type and *gad* mice on various postnatal days. In each group, the data represent the mean ± SD (n = 4; * $P < 0.05$). B) The extent of apoptosis in 2-wk-old mice. i, wild-type mice; ii, *gad* mice. Green fluorescence, TUNEL-positive cells; red fluorescence, nuclei stained with propidium iodide. Magnification ×100. Bar = 30 μm.

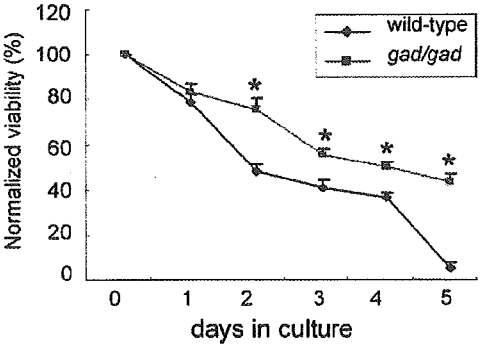

FIG. 4. In vitro survival of testicular germ cells. Testicular germ cells were isolated from wild-type and *gad* mice at 14 days of age. After culture, viability was determined using a Vi-Cell XR cell viability analyzer (Beckman Coulter). Viability at each time point was normalized to that at Day 0. Each data point represents the mean ± SD (n = 4; * $P < 0.05$).

Levels of Apoptotic Proteins During the First Round of Spermatogenesis

Germ cell apoptosis involves genes encoding various factors, such as *Trp53*, the *Bcl2* family, and *caspase*, which are targets for ubiquitination [29–31]. Our previous work demonstrated that the expression of antiapoptotic proteins (Bcl2 family and XIAP) is significantly elevated following cryptorchid stress in *gad* mice [22]. To explore whether the germ cell apoptotic wave is associated with changes in the levels of proteins known to be associated with cell death or survival, Western blot analysis was performed on testicular lysates obtained from 7-, 14-, 21-, 28-, and 35-day-old wild-type and *gad* mice (Fig. 5). Levels of TRP53 and Bax proteins were strikingly elevated in 7-day-old mice but barely detectable on Day 35. Caspase-3 was also strikingly elevated in 7-day-old mice. Since TRP53 modulates Bax expression [22, 32], the observed up-regulation of Bax is consistent with elevated TRP53 levels during the early apoptotic wave. Expression of the antiapoptotic protein Bcl-xL was weaker in immature compared with mature testes. Levels of TRP53, Bax, and caspase-3 proteins were significantly decreased in 7- and 14-day-old *gad* mice relative to the levels observed in wild-type testes (Fig. 5B). By contrast, the level of Bcl-xL protein appeared to be up-regulated earlier in *gad* mice (at 28 days) than in wild-type mice (at 35 days) (Fig. 5B).

Assessment of Cauda Epididymidis and Spermatozoa Morphology in gad *Mice*

The cauda epididymidis from wild-type and *gad* mice were weighed, and the sperm were collected and analyzed. The cauda epididymidis from *gad* mice weighed significantly less, likely resulting from the lower sperm concentration measured in *gad* mice (19.5×10^6/ml) compared with wild-type mice (23.6×10^6/ml) (Table 1). Furthermore, abnormal sperm morphology, including head and midpiece defects or a detached head, occurred significantly more often in *gad* mice (Table 1 and Fig. 6A). Immunocytochemical analysis showed that UCHL1 and ubiquitin were expressed in defective spermatozoa but not in normal spermatozoa (Fig. 6B). Ubiquitin, a marker for sperm abnormalities [33], was detected mainly in defective spermatozoa. However, despite a significantly elevated number of defective spermatozoa, ubiquitin expression in *gad* mouse spermatozoa was similar to that in wild-type mice (data not shown).

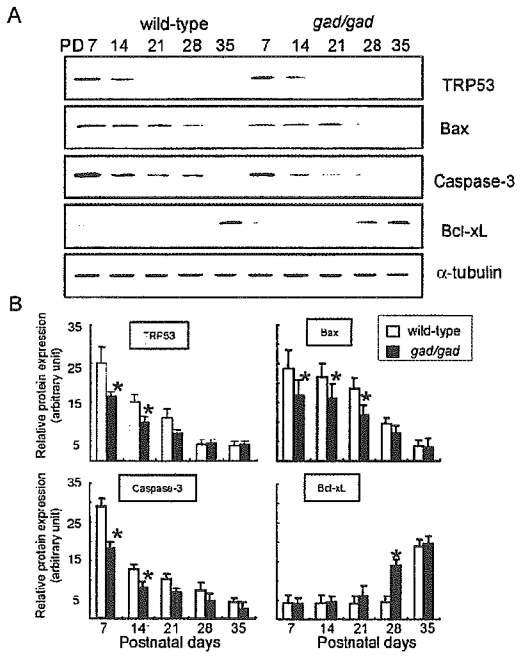

FIG. 5. A) Western blot analyses showing TRP53, Bax, caspase-3, and Bcl-xL levels in wild-type and *gad* mice during the first round of spermatogenesis. Protein (5 μg/lane) was prepared from whole testes at 7, 14, 21, 28, and 35 days of age. Blots were reprobed for α-tubulin to normalize for differences in the amount of protein loaded. Representative images of four independent experiments are shown. B) Quantitative Western blot analysis of changes in TRP53, Bax, caspase-3, and Bcl-xL levels. Relative protein expression (optical density) of the bands in panel A, normalized to α-tubulin. Each data point represents the mean ± SD (n = 4; * $P < 0.05$).

TABLE 1. Analysis of epididymal tail weight and sperm morphology (mean ± SD) in 10-week-old wild-type and *gad* mice.

	Tail weight (mg)	Sperm concentration (10^6/ml)	Defect (%)			
			Head	Midpiece	Principal piece	Detached head
wild-type	30.0 ± 0.8	23.6 ± 3.7	7.2 ± 1.5	2.4 ± 1.3	1.1 ± 0.2	2.0 ± 1.0
gad/gad	24.7 ± 1.1*	19.5 ± 3.3*	14.1 ± 2.8*	4.7 ± 1.5*	1.7 ± 0.6	3.7 ± 1.2*

* Significantly different from wild-type mice (n = 7; $P < 0.05$).

Spermatozoa Motility in gad *Mice*

We measured sperm motility parameters in wild-type and *gad* mice. Of the parameters assessed, MSP, PMP, VAP (μm/sec), VSL (μm/sec), and VCL (μm/sec) were significantly lower in *gad* mice. ALH (μm), linearity (%), and straightness (%) did not differ significantly between *gad* and wild-type mice (Fig. 7). Of the parameters we measured, the number of PMP differed most significantly between *gad* mice (24.4%) and wild-type mice (34.3%) (Fig. 7A).

DISCUSSION

Spermatogenesis is a highly complex process involving male germ cell proliferation and maturation from spermatogonia to spermatozoa [34]. Apoptosis is common during this process and is believed to play an important role in controlling germ cell numbers and eliminating defective germ cells that carry DNA mutations, thus ensuring the production of intact, functional spermatozoa [35–37]. Normally, germ cells are extremely sensitive to DNA damage, as such lesions are incompatible with the ultimate function of these cells [23, 24, 37]. The early apoptotic wave may result in early elimination of defective germ cells in which DNA alterations have occurred through chromosomal crossing over during the first meiotic division [23, 24, 37].

Several lines of evidence indicate that UCHL1 associates with monoubiquitin and that the monoubiquitin pool is reduced in *gad* mice relative to wild-type mice [18, 19, 22]. Furthermore, testes from UCHL1-deficient *gad* mice [22] and mice carrying the K48R mutation in ubiquitin [38] show resistance to cryptorchid-induced apoptosis, suggesting that ubiquitin is critical for modulating testicular germ cell death. Normally, damaged proteins are polyubiquitinated and degraded via the ubiquitin-proteasome system; however, if damaged proteins are not degraded as easily when monoubiquitin is either mutated or reduced [22, 38], then germinal cells may become resistant to programmed death. Our results with the *gad* mouse suggest that ubiquitin induction is important for regulating programmed germinal cell death that is normally observed during the first round of spermatogenesis. We have now shown that immature testes from *gad* mice are resistant to the massive wave of germinal cell apoptosis during the first round of spermatogenesis. The increased resistance of UCHL1-deficient germ cells to apoptosis-inducing conditions in vivo and in vitro suggests that UCHL1 is involved in spermatogenesis (Figs. 3 and 4). The activity of the ubiquitin-proteasome system may be required for specific transitions between multiple developmental cellular processes and sequential apoptosis during spermatogenesis [6, 7, 39]. In addition, the ubiquitin-proteasome system is required for the degradation or modification of numerous germ cell-specific proteins during different phases of spermatogenesis [39–41].

Early apoptosis in testicular germ cells is regulated by a complicated signal transduction pathway. The testes contain high levels of TRP53, Bcl2 family, and caspase-3 proteins, which are targets for ubiquitination [29–31, 42–45]. However, the involvement of the ubiquitin system in the regu-

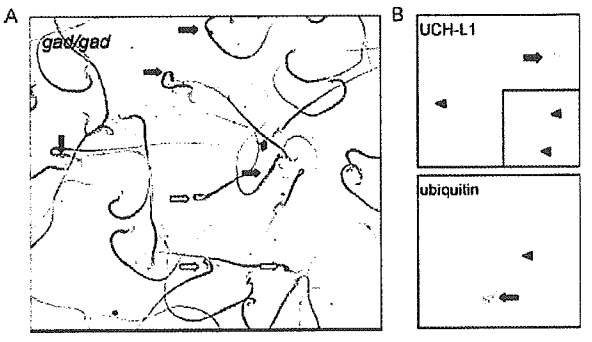

FIG. 6. A) Abnormal morphology of spermatozoa from *gad* mice. Spermatozoa were collected from the cauda epididymidis of 10-wk-old *gad* mice. Head defects (open arrows) and midpiece defects (closed arrows) are indicated. Magnification ×400. B) Immunocytochemistry of UCH-L1 and ubiquitin in wild-type and *gad* mice. UCHL1- and ubiquitin-positive spermatozoa (closed arrows) and normal spermatozoa (both negative, arrowheads) in wild-type mice are indicated. The inset shows an the image of spermatozoa from *gad* mice. Magnification ×1000.

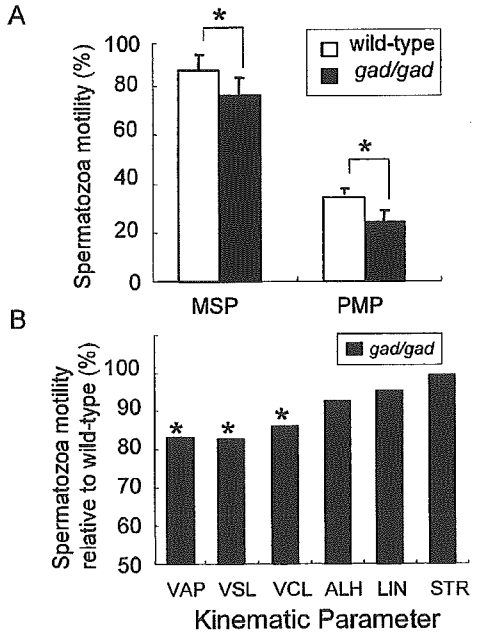

FIG. 7. Kinematic analysis of spermatozoa from the cauda epididymidis of 10-week-old wild-type and *gad* mice. A) Sperm motility. MSP, Percentage of motile sperm; PMP, Percentage of progressively motile sperm (n = 7; * $P < 0.05$). Data represent the mean ± SD. B) Movement characterization. VAP, Average path velocity (μm/sec); VSL, Straight-line velocity (μm/sec); VCL, Curvilinear velocity (μm/sec); ALH, Lateral head displacement (μm); LIN, Linearity (VSL/VCL × 100); STR, Straightness (VSL/VAP × 100). Data are expressed as a percentage of the values obtained for each parameter in wild-type mice (n = 7; * $P < 0.05$).

latory mechanisms of germ cell apoptosis has not been identified. A previous study showed that UCHL1-deficient *gad* mice express high levels of antiapoptotic proteins (Bcl2 family and XIAP) in the testis following cryptorchid-induced stress [22]. Alterations in the carefully maintained balance between the expression of apoptosis-inducing and apoptosis-protecting proteins may constitute one mechanism underlying the suppression of germ cell apoptosis observed in *gad* mice [46]. The decreased levels of TRP53, Bax, and caspase-3 observed in *gad* mice in this study are consistent with the suppression of germ cell apoptosis. In addition, the expression of the antiapoptotic protein Bcl-xL increased earlier in *gad* mice compared with wild-type mice. Therefore, the control of the apoptotic wave probably depends on variations in the balance between Bax and Bcl-xL [23, 47]. Analysis of the first round of spermatogenesis over time demonstrated a striking and massive wave of apoptotic germinal cells in 14-day-old mice (Fig. 3). High levels of UCHL1 protein were also observed at this age (Fig. 1) [20]. This early apoptotic wave was suppressed in the testes of *gad* mice, which had an abundance of germ cells compared with wild-type mice (Fig. 2). Moreover, the suppression of germ cell death is consistent with our previous report on cryptorchid stress injury in *gad* mice [22]. The testes of *gad* mice showed a phenotype similar to that of *Bax*-deficient mice or those overexpressing *Bcl2* or *Bcl-xL* [23, 25, 26]. Also, the testes of *Trp53*$^{-/-}$ mice exhibited a similar phenotype involving decreased germ cell apoptosis and an increased number of germ cells [48].

In the present study, we also characterized spermatozoa in *gad* mice with regard to the following reproductive endpoints: 1) the weight of reproductive organs, 2) the concentration of sperm cells, and 3) the motility and morphology of spermatozoa collected from the cauda epididymidis. The weight of cauda epididymidis from *gad* mice was significantly lower compared with that from wild-type mice. The concentration of sperm cells was also significantly lower, and most motility parameters of spermatozoa collected from the cauda epididymidis were affected in *gad* mice (Fig. 7). The significant decline in progressive forward motility, VAP, VSL, and VCL indicates that UCHL1 deficiency affects not only the ability of spermatozoa to move in the forward direction but also their vigor. In addition, the percentage of morphologically abnormal spermatozoa was significantly higher in *gad* mice (Table 1 and Fig. 6A).

Sperm production in the testis is a regulated balance between germ cell division and germ cell loss [26, 49], and there is emerging evidence that the ubiquitin-proteasome system may be central to the coordination of this process. For example, during spermatogenesis, the general activity of the ubiquitin-proteasome system is high, probably reflecting the requirement for massive degradation of cytoplasmic and nuclear proteins [6, 7, 50, 51]. Additionally, mutation of the ubiquitin-conjugating enzyme HR6B results in impaired spermatogenesis during nuclear condensation in spermatids [39, 41]. We found the fact that UCH-L1 associates with monoubiquitin in several lines of *gad* mice [18, 19, 22]. Furthermore, both proteins are expressed abundantly and at comparable levels in testis and the epididymis [11, 13, 14], suggesting that the functions of two proteins are important during spermatogenesis. Ubiquitin is present in defective spermatozoa, and proteins in these cells become ubiquitinated during epididymal passage (Fig. 6B) [11, 14, 33, 52, 53]. Furthermore, ubiquitination in the epididymis may trigger apoptotic mechanisms that recognize and eliminate abnormal spermatozoa [49, 54, 55].

Further study is required to elucidate the functional significance of the association between UCHL1 and ubiquitin during spermatozoa maturation in the epididymis. However, our observations suggest that UCHL1 may function to regulate sperm production and to ubiquitinate proteins in defective spermatozoa. Our present study demonstrates that UCHL1-deficient *gad* mice are resistant to the wave of germinal cell apoptosis that occurs during the first round of spermatogenesis and that these mice have defects in sperm production, motility, and morphology. These results suggest that UCHL1 functions in the early apoptotic wave during the first round of spermatogenesis and in the control of sperm quality during sperm maturation.

ACKNOWLEDGMENTS

We thank H. Kikuchi for technical assistance with tissue sections and M. Shikama for the care and breeding of animals.

REFERENCES

1. Ciechanover A, Finley D, Varshavsky A. Ubiquitin dependence of selective protein degradation demonstrated in the mammalian cell cycle mutant ts85. Cell 1984; 37:57–66.
2. Glotzer M, Murray AW, Kirschner MW. Cyclin is degraded by the ubiquitin pathway. Nature 1991; 349:132–138.
3. Strous GJ, Govers R. The ubiquitin-proteasome system and endocytosis. J Cell Sci 1999; 112(pt 10):1417–1423.
4. Wilkinson KD. Regulation of ubiquitin-dependent processes by deubiquitinating enzymes. FASEB J 1997; 11:1245–1256.
5. Hershko A, Ciechanover A. The ubiquitin system. Annu Rev Biochem 1998; 67:425–479.
6. Baarends WM, Roest HP, Grootegoed JA. The ubiquitin system in gametogenesis. Mol Cell Endocrinol 1999; 151:5–16.
7. Baarends WM, van der Laan R, Grootegoed JA. Specific aspects of the ubiquitin system in spermatogenesis. J Endocrinol Invest 2000; 23:597–604.
8. Ciechanover A. The ubiquitin-proteasome pathway: on protein death and cell life. EMBO J 1998; 17:7151–7160.
9. Weissman AM. Themes and variations on ubiquitylation. Nat Rev Mol Cell Biol 2001; 2:169–178.
10. Wing SS. Deubiquitinating enzymes—the importance of driving in reverse along the ubiquitin-proteasome pathway. Int J Biochem Cell Biol 2003; 35:590–605.
11. Fraile B, Martin R, De Miguel MP, Arenas MI, Bethencourt FR, Peinado F, Paniagua R, Santamaria L. Light and electron microscopic immunohistochemical localization of protein gene product 9.5 and ubiquitin immunoreactivities in the human epididymis and vas deferens. Biol Reprod 1996; 55:291–297.
12. Kon Y, Endoh D, Iwanaga T. Expression of protein gene product 9.5, a neuronal ubiquitin C-terminal hydrolase, and its developing change in sertoli cells of mouse testis. Mol Reprod Dev 1999; 54:333–341.
13. Kwon J, Kikuchi T, Setsuie R, Ishii Y, Kyuwa S, Yoshikawa Y. Characterization of the testis in congenitally ubiquitin carboxy-terminal hydrolase-1 (Uch-L1) defective (gad) mice. Exp Anim 2003; 52:1–9.
14. Martin R, Santamaria L, Fraile B, Paniagua R, Polak JM. Ultrastructural localization of PGP 9.5 and ubiquitin immunoreactivities in rat ductus epididymidis epithelium. Histochem J 1995; 27:431–439.
15. Pickart CM, Rose IA. Ubiquitin carboxyl-terminal hydrolase acts on ubiquitin carboxyl-terminal amides. J Biol Chem 1985; 260:7903–7910.
16. Liu Y, Fallon L, Lashuel HA, Liu Z, Lansbury PT, Jr. The UCH-L1 gene encodes two opposing enzymatic activities that affect alpha-synuclein degradation and Parkinson's disease susceptibility. Cell 2002; 111:209–218.
17. Liu Y, Lashuel HA, Choi S, Xing X, Case A, Ni J, Yeh LA, Cuny GD, Stein RL, Lansbury PT, Jr. Discovery of inhibitors that elucidate the role of UCH-L1 activity in the H1299 lung cancer cell line. Chem Biol 2003; 10:837–846.
18. Osaka H, Wang YL, Takada K, Takizawa S, Setsuie R, Li H, Sato Y, Nishikawa K, Sun YJ, Sakurai M, Harada T, Hara Y, Kimura I, Chiba S, Namikawa K, Kiyama H, Noda M, Aoki S, Wada K. Ubiquitin carboxy-terminal hydrolase L1 binds to and stabilizes monoubiquitin in neuron. Hum Mol Genet 2003; 12:1945–1958.

19. Harada T, Harada C, Wang YL, Osaka H, Amanai K, Tanaka K, Takizawa S, Setsuie R, Sakurai M, Sato Y, Noda M, Wada K. Role of ubiquitin carboxy terminal hydrolase-L1 in neural cell apoptosis induced by ischemic retinal injury in vivo. Am J Pathol 2004; 164:59–64.
20. Kwon J, Wang YL, Setsuie R, Sekiguchi S, Sakurai M, Sato Y, Lee WW, Ishii Y, Kyuwa S, Noda M, Wada K, Yoshikawa Y. Developmental regulation of ubiquitin C-terminal hydrolase isozyme expression during spermatogenesis in mice. Biol Reprod 2004; 71:515–521.
21. Saigoh K, Wang YL, Suh JG, Yamanishi T, Sakai Y, Kiyosawa H, Harada T, Ichihara N, Wakana S, Kikuchi T, Wada K. Intragenic deletion in the gene encoding ubiquitin carboxy-terminal hydrolase in gad mice. Nat Genet 1999; 23:47–51.
22. Kwon J, Wang YL, Setsuie R, Sekiguchi S, Sato Y, Sakurai M, Noda M, Aoki S, Yoshikawa Y, Wada K. Two closely related ubiquitin C-terminal hydrolase isozymes function as reciprocal modulators of germ cell apoptosis in cryptorchid testis. Am J Pathol 2004; 165: 1367–1374.
23. Rodriguez I, Ody C, Araki K, Garcia I, Vassalli P. An early and massive wave of germinal cell apoptosis is required for the development of functional spermatogenesis. EMBO J 1997; 16:2262–2270.
24. Jahnukainen K, Chrysis D, Hou M, Parvinen M, Eksborg S, Soder O. Increased apoptosis occuring during the first wave of spermatogenesis is stage-specific and primarily affects midpachytene spermatocytes in the rat testis. Biol Reprod 2004; 70:290–296.
25. Furuchi T, Masuko K, Nishimune Y, Obinata M, Matsui Y. Inhibition of testicular germ cell apoptosis and differentiation in mice misexpressing Bcl-2 in spermatogonia. Development 1996; 122:1703–1709.
26. Russell LD, Chiarini-Garcia H, Korsmeyer SJ, Knudson CM. Bax-dependent spermatogonia apoptosis is required for testicular development and spermatogenesis. Biol Reprod 2002; 66:950–958.
27. Slott VL, Suarez JD, Perreault SD. Rat sperm motility analysis: methodologic considerations. Reprod Toxicol 1991; 5:449–458.
28. Goyal HO, Braden TD, Mansour M, Williams CS, Kamaleldin A, Srivastava KK. Diethylstilbestrol-treated adult rats with altered epididymal sperm numbers and sperm motility parameters, but without alterations in sperm production and sperm morphology. Biol Reprod 2001; 64:927–934.
29. Chipuk JE, Green DR. Cytoplasmic p53: Bax and forward. Cell Cycle 2004; 3:429–431.
30. Dimmeler S, Breitschopf K, Haendeler J, Zeiher AM. Dephosphorylation targets Bcl-2 for ubiquitin-dependent degradation: a link between the apoptosome and the proteasome pathway. J Exp Med 1999; 189:1815–1822.
31. Suzuki Y, Nakabayashi Y, Takahashi R. Ubiquitin-protein ligase activity of X-linked inhibitor of apoptosis protein promotes proteasomal degradation of caspase-3 and enhances its anti-apoptotic effect in Fas-induced cell death. Proc Natl Acad Sci U S A 2001; 98:8662–8667.
32. Selvakumaran M, Lin HK, Miyashita T, Wang HG, Krajewski S, Reed JC, Hoffman B, Liebermann D. Immediate early upregulation of bax expression by p53 but not TGF beta 1: a paradigm for distinct apoptotic pathways. Oncogene 1994; 9:1791–1798.
33. Sutovsky P, Moreno R, Ramalho-Santos J, Dominko T, Thompson WE, Schatten G. A putative, ubiquitin-dependent mechanism for the recognition and elimination of defective spermatozoa in the mammalian epididymis. J Cell Sci 2001; 114:1665–1675.
34. de Kretser DM, Loveland KL, Meinhardt A, Simorangkir D, Wreford N. Spermatogenesis. Hum Reprod 1998; 13(suppl 1):1–8.
35. Gosden R, Spears N. Programmed cell death in the reproductive system. Br Med Bull 1997; 53:644–661.
36. Matsui Y. Regulation of germ cell death in mammalian gonads. APMIS 1998; 106:142–147Ascussion 147–148.
37. Print CG, Loveland KL. Germ cell suicide: new insights into apoptosis during spermatogenesis. Bioessays 2000; 22:423–430.
38. Rasoulpour RJ, Schoenfeld HA, Gray DA, Boekelheide K. Expression of a K48R mutant ubiquitin protects mouse testis from cryptorchid injury and aging. Am J Pathol 2003; 163:2595–2603.
39. Baarends WM, Wassenaar E, Hoogerbrugge JW, van Cappellen G, Roest HP, Vreeburg J, Ooms M, Hoeijmakers JH, Grootegoed JA. Loss of HR6B ubiquitin-conjugating activity results in damaged synaptonemal complex structure and increased crossing-over frequency during the male meiotic prophase. Mol Cell Biol 2003; 23:1151–1162.
40. Baarends WM, Hoogerbrugge JW, Roest HP, Ooms M, Vreeburg J, Hoeijmakers JH, Grootegoed JA. Histone ubiquitination and chromatin remodeling in mouse spermatogenesis. Dev Biol 1999; 207: 322–333.
41. Roest HP, van Klaveren J, de Wit J, van Gurp CG, Koken MH, Vermey M, van Roijen JH, Hoogerbrugge JW, Vreeburg JT, Baarends WM, Bootsma D, Grootegoed JA, Hoeijmakers JH. Inactivation of the HR6B ubiquitin-conjugating DNA repair enzyme in mice causes male sterility associated with chromatin modification. Cell 1996; 86: 799–810.
42. Marshansky V, Wang X, Bertrand R, Luo H, Duguid W, Chinnadurai G, Kanaan N, Vu MD, Wu J. Proteasomes modulate balance among proapoptotic and antiapoptotic Bcl-2 family members and compromise functioning of the electron transport chain in leukemic cells. J Immunol 2001; 166:3130–3142.
43. Oren M. Regulation of the p53 tumor suppressor protein. J Biol Chem 1999; 274:36031–36034.
44. Orlowski RZ. The role of the ubiquitin-proteasome pathway in apoptosis. Cell Death Differ 1999; 6:303–313.
45. Yang Y, Yu X. Regulation of apoptosis: the ubiquitous way. FASEB J 2003; 17:790–799.
46. Beumer TL, Roepers-Gajadien HL, Gademan IS, Lock TM, Kal HB, De Rooij DG. Apoptosis regulation in the testis: involvement of Bcl-2 family members. Mol Reprod Dev 2000; 56:353–359.
47. Borner C. The Bcl-2 protein family: sensors and checkpoints for life-or-death decisions. Mol Immunol 2003; 39:615–647.
48. Yin Y, Stahl BC, DeWolf WC, Morgentaler A. p53-mediated germ cell quality control in spermatogenesis. Dev Biol 1998; 204:165–171.
49. Sutovsky P. Ubiquitin-dependent proteolysis in mammalian spermatogenesis, fertilization, and sperm quality control: killing three birds with one stone. Microsc Res Tech 2003; 61:88–102.
50. Rajapurohitam V, Bedard N, Wing SS. Control of ubiquitination of proteins in rat tissues by ubiquitin conjugating enzymes and isopeptidases. Am J Physiol Endocrinol Metab 2002; 282:E739–E745.
51. Rajapurohitam V, Morales CR, El-Alfy M, Lefrancois S, Bedard N, Wing SS. Activation of a UBC4-dependent pathway of ubiquitin conjugation during postnatal development of the rat testis. Dev Biol 1999; 212:217–228.
52. Lippert TH, Seeger H, Schieferstein G, Voelter W. Immunoreactive ubiquitin in human seminal plasma. J Androl 1993; 14:130–131.
53. Sutovsky P, Terada Y, Schatten G. Ubiquitin-based sperm assay for the diagnosis of male factor infertility. Hum Reprod 2001; 16:250–258.
54. Sinha Hikim AP, Swerdloff RS. Hormonal and genetic control of germ cell apoptosis in the testis. Rev Reprod 1999; 4:38–47.
55. Sutovsky P, Hauser R, Sutovsky M. Increased levels of sperm ubiquitin correlate with semen quality in men from an andrology laboratory clinic population. Hum Reprod 2004; 19:628–638.

Available online at www.sciencedirect.com
SCIENCE DIRECT
Developmental Biology 281 (2005) 196–207
DEVELOPMENTAL BIOLOGY
www.elsevier.com/locate/ydbio

Dynamic rearrangement of telomeres during spermatogenesis in mice

Kentaro Tanemura[a], Atsuo Ogura[b], Cheolho Cheong[c], Hideo Gotoh[d], Kazuya Matsumoto[e], Eimei Sato[f], Yoshihiro Hayashi[g], Han-Woong Lee[c], Takashi Kondo[a,*]

[a]*Brain Development Research Group, Brain Science Institute, Institute of Physical and Chemical Research (RIKEN), 2-1 Hirosawa, Wako, Saitama 351-0198, Japan*
[b]*Bioresource Center, RIKEN, Tsukuba, Ibaraki 305-0074, Japan*
[c]*Department of Molecular Cell Biology, Sungkyunkwan University School of Medicine and Samsung Biomedical Research Institute, Suwon 440-746, Korea*
[d]*Experimental Animals Laboratory, Molecular Biology and Immunology Department, National Institute of Agrobiological Sciences, Tsukuba, Ibaraki 305-8602, Japan*
[e]*Department of Genetic Engineering, Kinki University, Nagagun, Wakayama 649-6493, Japan*
[f]*Laboratory of Animal Reproduction, Graduate School of Agricultural Science, Tohoku University, Sendai, Miyagi 981-8555, Japan*
[g]*Laboratory of Global Animal Science, Graduate School of Agricultural and Life Sciences, The University of Tokyo, Tokyo 113-8657, Japan*

Received for publication 8 October 2004, revised 10 February 2005, accepted 23 February 2005
Available online 30 March 2005

Abstract

Chromosomal structure within the nucleus influences various biological processes such as transcription and replication. Telomeres are located at the end of eukaryotic chromosomes and they can be a decisive factor for correct chromosomal positioning. To gain new insight into telomere dynamics, we examined telomere length and positional changes during spermatogenesis using improved fluorescence in situ hybridization (FISH) and in situ telomeric repeat amplification protocols (TRAP) on histological sections. FISH revealed telomere length and chromosome position within nuclei change dynamically. Telomere extension occurred during spermiogenesis. In situ TRAP analysis verified elevated telomerase activity in elongating spermatids. Together, these data show that elongated spermatids have longer telomeres than precursor spermatogenic cells. This observation indicates that telomere elongation in haploid cells occurs after meiosis and in the absence of genomic replication. Analyses of testes from telomerase null mice further support the significance of telomere dynamics during spermatogenesis and the existence of an alternative telomere extension pathway.

Keywords: Telomere; Telomerase; FISH; TRAP assay; Mouse; Spermatogenesis

Introduction

Telomeres are DNA–protein complexes located at the ends of linear eukaryotic chromosomes. They protect chromosomes from terminal fusions or degradation that typically occurs during the DNA replication cycle, and thus, are essential for genomic and genetic stability of cells (de Lange, 2002; Ducray et al., 1999; Felder et al., 2003; Greider, 1996; Wong and Collins, 2003). In mammals, telomere DNA contains tandem repeats of a hexanucleotide (TTAGGG) sequence. The number of telomeric repeats (telomere length) is known to be important for inheritance of genomic structure and is primarily maintained by telomerase activity during the cell cycle. Mammalian telomerase is a protein–RNA complex composed of a catalytic subunit, telomerase reverse transcriptase (*Terc*; Blasco et al., 1995), and a telomerase RNA component (*Tert*; Nakamura et al., 1997) that directs the addition of telomeric repeat sequences to the end of the chromosome. Since telomerase activity is progressively down-regulated during terminal differentiation, the reduction of telomeric repeats can be observed during the normal development of

* Corresponding author. Fax: +81 48 467 6729.
E-mail address: TKondo@brain.riken.go.jp (T. Kondo).

0012-1606/$ - see front matter © 2005 Elsevier Inc. All rights reserved.
doi:10.1016/j.ydbio.2005.02.025

somatic tissues (Greenberg et al., 1998; Greider and Blackburn, 1996; Prowse and Greider, 1995). Telomerase null (*Terc*$^{-/-}$) mice exhibit decreased fertility, progressive defects in several organs, and shortened life span after several generations because of telomere shortening (Blasco et al., 1997; Lee et al., 1998). On the other hand, cells that acquire immortality like cancer, maintain telomerase activity and avoid telomere loss, even after multiple rounds of cell division (Hiyama and Hiyama, 2002). In general, sufficient telomere length must be maintained for cells to continually proliferate and to sidestep cellular senescence. Thus, telomerase activity is required to ensure that genomic structure is properly maintained during successive cycles of reproduction and development in eukaryotes.

Extensive studies in yeast have revealed that telomeres are responsible for conveying important positional cues for chromatin formation and arrangement within nuclei. These arrangements significantly affect transcription regulation and cellular proliferation (Andrulis et al., 1998; Gasser, 2002). Telomeres gather in peripheral regions of the nucleus where they form several clusters (Gotta et al., 1996), silencing genes at subtelomeric regions (Guarente, 1999). In mammals, the spatial arrangement of chromosomes is also important (Cremer and Cremer, 2001; Dietzel and Belmont, 2001; Gerlich et al., 2003; Grosveld, 1999). Although telomere position most likely is regulated according to developmental phase, the significance of these positional cues remains unclear in higher eukaryotes.

To study the higher organization of nuclear and chromosome structure, we improved the Q-FISH (quantitative fluorescence in situ hybridization) technique, which enabled us to simultaneously observe the localization and the quantity of telomeres within histological sections (Meeker et al., 2002). In addition, we developed an in situ TRAP assay, which allowed us to detect telomere extension activity in histological sections with single-cell resolution. This assay can be used diagnostically to detect the early appearance of immortal cells in organs. In the present study, we used these techniques to observe telomere dynamics during spermatogenesis, a process in which telomere dynamics is relatively well known.

In mice, spermatogenesis undertake within seminiferous tubule and can be divided mainly into three phases according to cell state (Leblomd and Clermont, 1952)—proliferative, meiotic, and spermiogenic phases. During the proliferative phase, spermatogonial cells multiply via mitosis to form immature primary spermatocytes called preleptotene spermatocytes. In the meiotic phase, preleptotene spermatocytes undergo meiosis to produce leptotene, zygotene, pachytene, and finally diplotene spermatocytes; these cells are distinguishable by their chromosomal states. Meiotic DNA replication takes place in preleptotene spermatocytes and chromosomal unraveling takes place in leptotene spermatocytes. Homologous chromosomes pair up in zygotene spermatocytes and chromosomes thicken and recombine in pachytene spermatocytes. Diplotene spermatocytes undergo the first set of meiotic divisions to form secondary diploid spermatocytes, which further undergo a second meiotic division to generate spermatids. In the spermiogenic phase, these haploid spermatids mature into sperm after 16 steps of differentiation. Round spermatids form during steps 1–7, elongating spermatids during steps 8–12, elongated spermatids during steps 13–16, and finally mature sperm form (Russell et al., 1990). Cross-section of seminiferous epithelium shows specific combination of cells on the sperm maturation steps (Russell et al., 1990). A set of cell association by logical sequence of maturation step is defined as the cycle of seminiferous epithelium and 12 different stages of seminiferous epithelia are recognizable according to combination of maturing spermatogenic cells. A section of seminiferous epithelium contains specific spermatogenic cells in 3–4 different maturation steps, for example, stage I seminiferous epithelium contains early pachytene, step 1 round spermatids, and step 13 elongated spermatids (Russell et al., 1990).

In addition to confirming previous reports (Achi et al., 2000; Meyer-Ficca et al., 1998; Pfeifer et al., 2001; Scherthan et al., 1996; Zalenskaya and Zalensky, 2002, 2004), we found several novel aspects of telomere dynamics during spermatogenesis.

Materials and methods

Mice

Male C57/B6 mice (4 and 12 weeks of old), telomerase null mice (*Terc*$^{-/-}$ mice; FVB/N background; 8 months of old) and control mice (*Terc*$^{+/-}$ mice; FVB/N background; 8 months of old) were used. All mice were anesthetized with 2, 2, 2-tribromoethanol before using.

FISH analysis

Mouse testes were surgically taken out and fixed with methacarn fixative, embedded in paraffin, and sectioned. Cross-sections (10–25 μm) were deparaffinized then incubated at 90°C with pre-treatment citrate buffer (developed with Nacalai Tesque, Inc., Japan.) containing 10 mM EDTA, 0.05% NP40, and 0.05% Triton X-100. After washing, sections were denatured with 70% formamide/2 × SSC at 100°C for 3 min, dehydrated in cold ethanol for 3 min, incubated with 0.2 μg/ml rhodamine-labeled telomeric PNA probe of $(TTAGGG)_3$ in HYBRIDSOL VII (Oncor, USA) at 50°C for 12 h, and washed with 0.01× SSC at 50°C. Nuclei were counterstained with SYTE-Green (Molecular Probes, USA). Some sections were sequentially reacted with anti-PCNA monoclonal antibody (Oncogene Research Products, USA) and Alexa Fluor™ 633-labeled secondary antibody (Molecular Probes, USA). FISH images and immunostained images were obtained with an LSM-510 confocal laser microscope

(Carl Zeiss, Germany) by sequential scanning and analyzed with adjunctive software attached to the LSM-510.

Terminal restriction fragment (TRF) length analysis

Genomic DNA prepared from brain, liver, kidney, testis, and sperm of B6 male mice was digested for 16 h with *Hin*fI. A 10-μg sample of digested DNA was separated in 1% agarose gels with the CHEF-DR III pulse field system (Bio-Rad, UK), and separated DNAs were transferred onto positively charged membranes. The membrane was hybridized at 37°C to a biotin-labeled oligonucleotide probe of $(TTAGGG)_3$, and TRF length was detected by a LAS-3000 imaging system (Fuji Photo Film, Japan) using CSPD (Tropix, USA).

Quantitative analysis of FISH images

After adjusting background noise using the public domain NIH Image program (developed at the U.S. National Institutes of Health and available on the Internet at http://rsb.info.nih.gov/nih-image/), we calculated the fluorescence intensity of telomeres within each nucleus in the FISH images.

In situ TRAP assays

Mouse testes were surgically taken out and fresh adult mouse testes were embedded in O.C.T. compound and cross-sectioned into 4 μm-thick sections. Sections were dried for a few hours prior to incubation in telomerase reaction buffer (100 μl) containing 20 mM Tris–HCl (pH 8.3), 1.5 mM $MgCl_2$, 63 mM KCl, 1 mM EGTA, 50 μM dNTP, 0.1% bovine serum albumin, and TS-primer (5′-AAT CCG TCG AGC AGA GTT-3′). They were then fixed in a neutral buffered 10% formalin solution. Sections were washed with 0.01 M PBS, dehydrated, and dried. Elongation products were detected by PCR with dNTP containing digoxigenin-11-dUTP and a pair of TS- and CX-primers (5′-CCC TTA CCC TTA CCC TTA CCC TAA-3′). In situ PCR was performed with TaKaRa PCR Thermal Cycler MP and TaKaRa Slide Seal for in situ PCR (TaKaRa, Japan) in a final volume of 20 μl. Fifteen cycles of in situ PCR were carried out at 94°C for 30 s and at 60°C for 30 s. After washing with 0.01 M PBS, the sections were reacted with anti-digoxigenin-POD antibody (Roche Diagnostics, USA), and signals were visualized with 0.05% 3,3′-diaminobenzidine tetrahydrochloride in 0.01 M PBS and 0.01% H_2O_2. The sections were stained with hematoxylin for nuclear counterstaining.

Immunohistochemistry

Mouse testes were surgically taken out and fixed with methacarn fixative, embedded in paraffin, and sectioned. Cross-sections (4–5 μm) were deparaffinized, then incubated with anti-TERT (2C4) monoclonal antibody (Abcam, UK). Immunoreactive elements were visualized with Alexa Fluor™ 488-labeled secondary antibodies. Nuclei in some sections were counterstained with propidium iodide (Molecular Probes, USA). Stained images were obtained with an LSM-510 confocal laser microscope and analyzed with adjunctive software attached to the LSM-510.

Lectin histochemistry

Cross-sections (4–5 μm) were deparaffinized, then incubated with either biotin-labeled SBA lectin (HONEN, Japan), a legume lectin that specifically recognizes tetrameric GalNAc/Gal. Immunoreactive elements were visualized with Alexa Fluor™ 488-labeled streptavidin. Nuclei in some sections were counterstained with propidium iodide (Molecular Probes, USA). Stained images were obtained with an LSM-510 confocal laser microscope and analyzed with adjunctive software attached to the LSM-510.

Results

Dynamic behavior of telomeres during spermatogenesis

Laser scanning microscopy and fluorescence in situ hybridization (FISH) techniques have revealed quantitative information on telomere length and positional information of telomeres within the nucleus (Henderson et al., 1996; Molenaar et al., 2003). To study telomere dynamics during spermatogenesis, we performed FISH on testis sections using a rhodamine-labeled peptide-nucleic acid (PNA) telomeric probe. After the elongated spermatid stage, the chromosomes of late spermatogenic cells become tightly packed with protamine, a histone-like protein, and such compaction of chromatin probably prevents the hybridization of probes with protocols previously reported (data not shown; Franco et al., 2002; Gonzalez-Suarez et al., 2000; Meeker et al., 2002). We were able to improve hybridization by developing a new pre-treatment citrate buffer for our sections (Figs. 1A–X), and observe the dynamics of telomeres in seminiferous tubules (Figs. 1A–C), in seminiferous epithelia (Figs. 1D–R) and in individual spermatogenic cells (Figs. 1S–X).

Several reports have described the position of telomeres within the nucleus of spermatogenic cells. We have isolated testes from C57Bl/6 male mice in 12 weeks of age for our study. During proliferation and mid-meiotic phases (i.e., spermatogonia to leptotene spermatocyte stages), telomeres disperse throughout the nucleus (arrowheads in Figs. 1I, L, O, U). Later in the meiotic phase, during the early zygotene spermatocyte stage, telomeres temporarily move to one pole of the nucleus (data not shown; Franco et al., 2002) before spreading to all peripheral parts of the nucleus in the late zygotene spermatocyte stage (arrowhead in Fig. 1R; Franco et al., 2002). Immediately thereafter in the pachytene

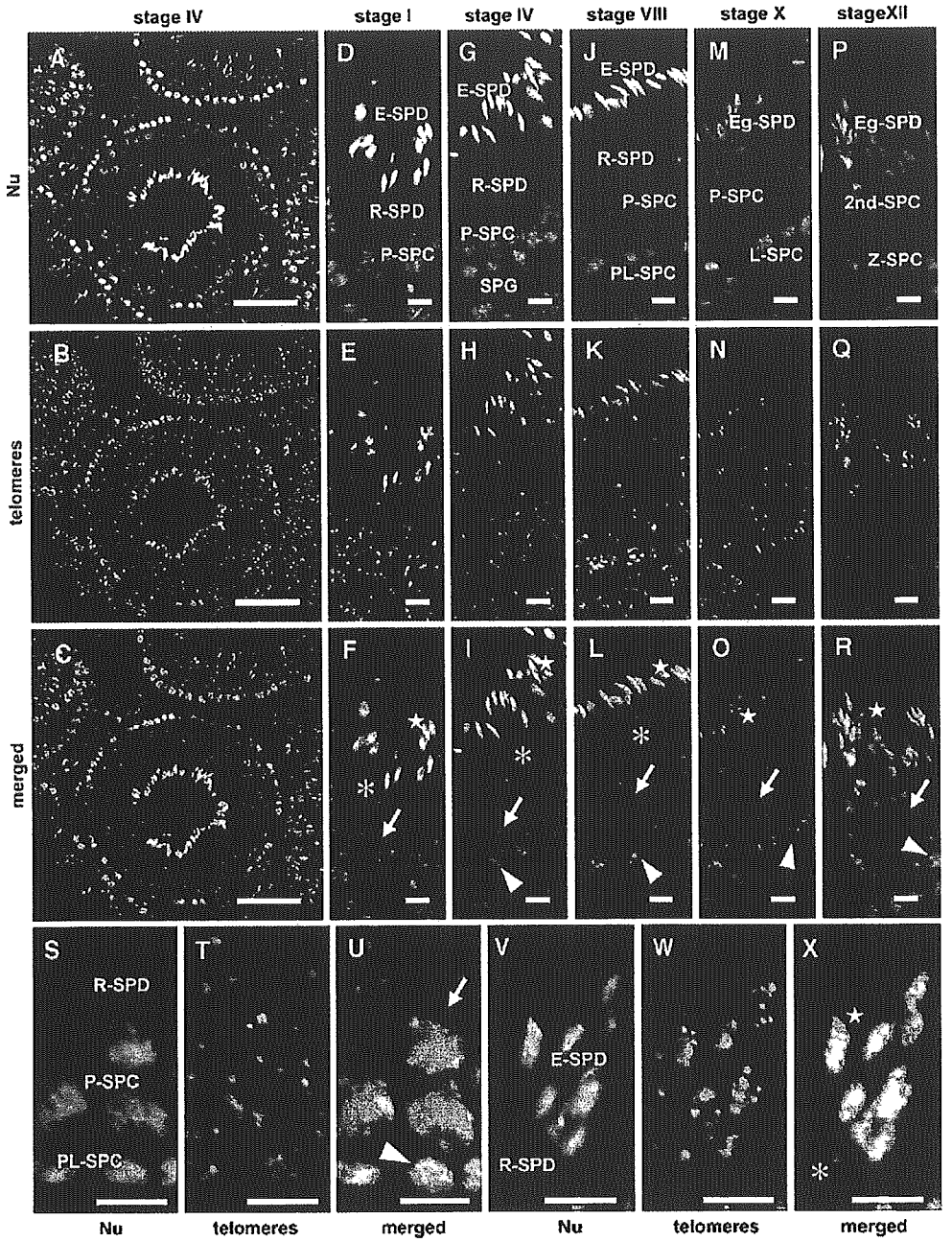

Fig. 1. FISH analysis of testis sections from sexually mature mice. (A, D, G, J, M, P, S, V) Signals represent nuclear counterstaining with SYTE-Green. (B, E, H, K, N, Q, T, W) Signals represent telomeres. (C, F, I, L, O, R, U, X) Merged images. Green signals represent nuclear counterstaining with SYTE-Green and red signals represent telomeres. (A–C) Images of seminiferous tubules at stage IV. (D–R) Images of seminiferous epithelia. (D–F) Seminiferous epithelia at stage I. Early pachytene spermatocytes (P-SPC indicated by arrow in F), step 1 round spermatids (R-SPD indicated by asterisk in F), and step 13 elongated spermatids (E-SPD indicated by star in F) are present. (G–I) Seminiferous epithelia at stage IV. Intermediate spermatogonia (SPG indicated by arrowhead in I), pachytene spermatocytes (P-SPC indicated by arrow in I), step 4 round spermatids (R-SPD indicated by asterisk in I), and step 15 elongated spermatids (E-SPD indicated by star in I) are present. (J–L) Seminiferous epithelia at stage VIII. Preleptotene spermatocytes (PL-SPC indicated by arrowhead in L), pachytene spermatocytes (P-SPC indicated by arrow in L), step 7 round spermatids (R-SPD indicated by asterisk in L), and step 16 elongated spermatids (E-SPD indicated by star in L) are present. (M–O) Seminiferous epithelia at stage X. Leptotene spermatocytes (L-SPC indicated by arrowhead in O), late pachytene spermatocytes (P-SPC indicated by arrow in O), and step 10 elongating spermatids (Eg-SPD indicated by star in O) are present. (P–R) Seminiferous epithelia at stage XII. Zygotene spermatocytes (Z-SPC indicated by arrow in R), secondary spermatocytes (2nd-SPC indicated by arrowhead in R), and step 12 elongating spermatids (Eg-SPD indicated by star in R) are present. (S–X) Highly magnified images of seminiferous epithelia. (S–U) Basement membrane side of seminiferous epithelia at stage VII. Preleptotene spermatocytes (PL-SPC indicated by arrowhead in indicated by U), pachytene spermatocytes (P-SPC indicated by arrow in U), and step 7 round spermatids (R-SPD) are present. (V–X) Lumen side of seminiferous epithelia at stage VII. Step 7 round spermatids (R-SPD indicated by asterisk in X) and step 16 elongated spermatids (E-SPD indicated by star in X) are present. (A–C) Scale bar = 50 μm. (D–X) Scale bar = 10 μm.

spermatocyte stage, telomeres remain in peripheral areas of the nucleus until the diplotene stage (arrows in Figs. 1F, I, L, O, U; Scherthan et al., 1996). In the secondary spermatocyte stage, telomeres leave the periphery (arrow in Fig. 1R). Then, in the round spermatid stage, most telomeres assemble around the nucleolus in the center of the nucleus (asterisks in Figs. 1F, I, L, X; Meyer-Ficca et al., 1998). After the elongating spermatid stage, telomeres disperse again (stars in Figs. 1F, I, L, R, X), simultaneously with the fading of the nucleolus. These observations are in good agreement with previous works (Meyer-Ficca et al., 1998; Pfeifer et al., 2001; Scherthan et al., 1996; Zalenskaya and Zalensky, 2002, 2004).

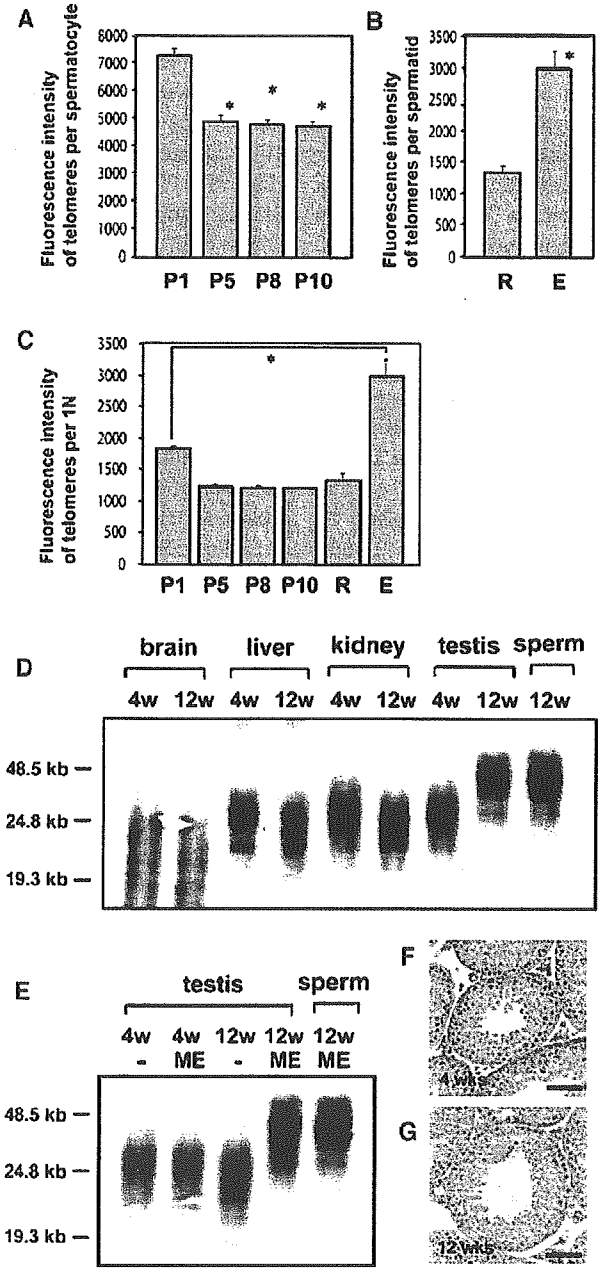

During spermatogenesis, dynamic rearrangements of telomeres are not restricted to changes only in position. Using this improved method, we found that the intensity of FISH signals representing individual telomeres started to decrease in pachytene spermatocytes (compare arrow in Fig. 1F and arrows in Figs. 1I, L, O) and remained low until the end of step 7 of spermiogenesis (i.e., round spermatid stage) (asterisks in Figs. 1F, I, L). Telomeric signals began to increase simultaneously with the elongation of spermatids (stars in Figs. 1O, R), and plateaued during the elongated spermatid stage (stars in Figs. 1F, I, L). Signal intensity most likely reflects the number of telomeric repeats in a cell; thus, signal intensity can also reflect the length of telomeres. Elongated spermatids, which are haploid cells, display more intense FISH signals than pachytene spermatocytes, which are tetraploid cells, indicating that elongated spermatids contain longer telomeres.

In summary, telomeres become shorter during the pachytene spermatocyte stage (arrows in Figs. 1F, I, L, O). During late spermatogenesis, telomeres began to extend (i.e., elongating spermatid stage) (stars in Figs. 1O, R) so that elongated spermatids possessed extremely long telomeres (stars in Figs. 1F, I, L). To investigate quantitative changes in telomere length, we measured the intensity of FISH signals in each cell type. In the nucleus of a pachytene spermatocyte located in the stage V seminiferous epithelium, telomeric signal intensity was about two thirds of that measured in pachytene spermatocytes located in stage I seminiferous epithelium; this intensity level remained unchanged through stage X (Fig. 2A). On the other hand, telomeric signal intensity of an elongated spermatid was about two times stronger than that of a round spermatid located in stage V seminiferous epithelium (Fig. 2B).

To compare the signal intensities measured in pachytene spermatocytes (4N) with those measured in spermatids (1N), we calculated a scaled intensity by dividing the intensities of pachytene spermatocytes by four; this scaled

Fig. 2. Quantitative analysis of FISH image and comparison of telomere length in tissues from immature and mature mice. (A) Telomeric signal intensity of individual pachytene spermatocytes in stages I (P1; n = 29), V (P5; n = 12), VIII (P8; n = 14), and X (P10; n = 11) seminiferous epithelia. (B) Telomeric signal intensity of individual round spermatids (R; n = 20) and individual elongated spermatids (E; n = 21) in stage V seminiferous epithelia. (C) Telomeric signal intensity of the haploid state. Individual pachytene spermatocytes in stages I (P1), V (P5), VIII (P8), and X (P10) seminiferous epithelia, and individual round spermatids (R) and individual elongated spermatids (E) in stage V seminiferous epithelia. *P < 0.01. (D) TRF length analysis of brain, liver, kidney, and testis from sexually immature (4 weeks of age) and young sexually mature (12 weeks of age; YM) mice, and of sperm from young sexually mature mice. (E) Effect of 2-ME on TRF length analysis of testes from a young sexually mature mouse. (F) Hematoxylin-stained testis section from an immature mouse. No elongated spermatids were observed in the seminiferous epithelia. (G) Hematoxylin-stained testis section from a mature mouse. All types of spermatogenic cells, including elongated spermatids, were detected in seminiferous epithelia. Active spermatogenesis was also observed. (F–G) Scale bar = 50 μm.

intensity corresponds to the signal intensity for haploid cells. This comparison indicated that decreased telomeric signal intensity in pachytene spermatocytes (in the stage V seminiferous epithelium) remained unchanged until the round spermatid phase. During the next stage of development, telomere extension occurred within elongating spermatids. As a result of this extension, FISH signals in elongated spermatids were about 2 times stronger than those in round spermatids and 1.5 times stronger than those in pachytene spermatocytes found in stage I seminiferous epithelium (Fig. 2C). We believe that the change of signal intensity did not result from variable probe accessibility to different cell types by two reasons. First, decrease of signal intensity occurs within pachytene spermatocyte phase, between pachytene spermatocytes from stage I and stage V seminiferous tubule, and chromatin structure does not change through these stages. Second, the signal intensity measured from the pachytene spermatocyte phase of stage V seminiferous epithelium through the round spermatid phase were more or less equivalent, even though the nuclear structures of cells present during these phases were greatly altered. Importantly, these findings indicate that the telomeres of haploid cells elongate after meiosis and in the absence of genomic DNA replication.

It has already been reported that telomere length is maintained in germ cells by telomerase activity (Hastie et al., 1990). We tested the terminal restriction fragment (TRF) lengths of genomic DNA derived from various tissues, including male germ cells, from sexually immature (postnatal age of 4 weeks) and young sexually mature (12 weeks). Chromosomal DNA in elongated spermatid and sperm is tightly packed with protamines (sperm-specific histone-like proteins) and this highly condensed DNA resist against standard isolation protocol. Since protamines form complexes by disulfide bonds (Biggiogera et al., 1992) hydrolyzable by 2-mercaptoethanol (2-ME), we isolated DNA with 2-mercaptoethanol (2-ME)-treated tissues and measured TRFs with these DNA samples. In brain, liver, and kidney, telomeres slightly shortened with age or were nearly the same length (Fig. 2D), as previously reported (Prowse and Greider, 1995). On the other hand, telomeres from mature testes, which contained all types of spermatogenic cells (Fig. 2G), were longer than those from sexually immature testes (Fig. 2D), which lack elongated spermatids and mature sperm (Fig. 2F). In adult mice, we found mature sperm among cells that have longer telomeres. This agrees well with the observation that isolated sperm have long telomeres and that TRF hybridization signals localized only to these mature sperm in adult testes (Fig. 2D) (Hastie et al., 1990). As noted above, DNA samples from 2-ME untreated testes mainly composed by the DNA from spermatogonia to elongating spermatid and nearly lack DNA fraction from elongated spermatid and sperm, we next compared TRFs in DNA from untreated and 2-ME-treated testes. Though the TRFs from sexually immature mice were nearly the same length between untreated and 2-ME-treated testis, TRFs of 2-ME-treated testes exhibited longer than those from untreated testes from 12 weeks age adult mice (Fig. 2E). These results clearly indicate that telomere elongation takes place in elongating spermatids stage of adult testis, and agrees well above observations of telomere dynamics on seminiferous epithelia by FISH protocol (Figs. 1F, I, L).

Telomeres are considered to be the structural basis for chromosomal architecture and movement, and their rearrangement may be the driving force for sequential changes in chromosomal configuration that occur during cell division. During the zygotene stage of meiosis, chromosomes frequently adopt bouquet-like formations that rapidly disappear before the pachytene stage (Pfeifer et al., 2001, 2003). The appearance and disappearance of these bouquet-like structures correspond, respectively, to the assembling of telomeres at the pole of the nucleus and the subsequent dispersing of telomeres throughout the peripheral parts of the nucleus (Scherthan, 2001). After telomeres reduce in length, they leave the peripheral parts of the nucleus; this occurs in the transition from the diplotene to secondary spermatocyte stages (arrow in Fig. 1R). This suggests that telomere length importantly affects telomere movement. Chromosomal rearrangements have been suggested to be important for meiosis to complete properly.

Telomere extension activity in spermatogenesis

To assess enzymatic activity underlying telomere extension during the different stages of spermatogenesis, we developed an in situ TRAP assay that could be implemented using histological sections. This adaptation of the TRAP assay, a useful method for measuring telomerase activity (Kim et al., 1994), enabled us to observe enzymatic activities underlying telomere extension in individual cells. We detected clear signals in elongating spermatids (Fig. 3A), as well as in spermatogonia (Fig. 3B). Signal intensity, however, was greater in elongating spermatids, supporting our FISH findings that telomere extension occurs in these spermatids. Signals faded in the next phase of spermatogenesis and disappeared at the elongated spermatid stage (Fig. 3B). These results agreed well with our FISH results (stars in Figs. 1F, I, L, O, R, X, C and 2B, C and 5). We conclude that telomere rearrangements in haploid cells occur before protamine-mediated chromatin condensation (Biggiogera et al., 1992).

We also investigated telomerase catalytic subunit (TERT) expression immunohistochemically and found TERT-immunopositive signals in differentiated spermatogonia and in early spermatocytes, cell types that occur during proliferative phases. Because these phases occur before telomere shortening, these observations suggest that telomerase activity is required for maintaining telomere length in proliferative cells. We failed to observe TERT signals in cells during phases that contain pachytene spermatocytes and round spermatids. We detected TERT immunoreactivities in elongating spermatids at stage X of seminiferous

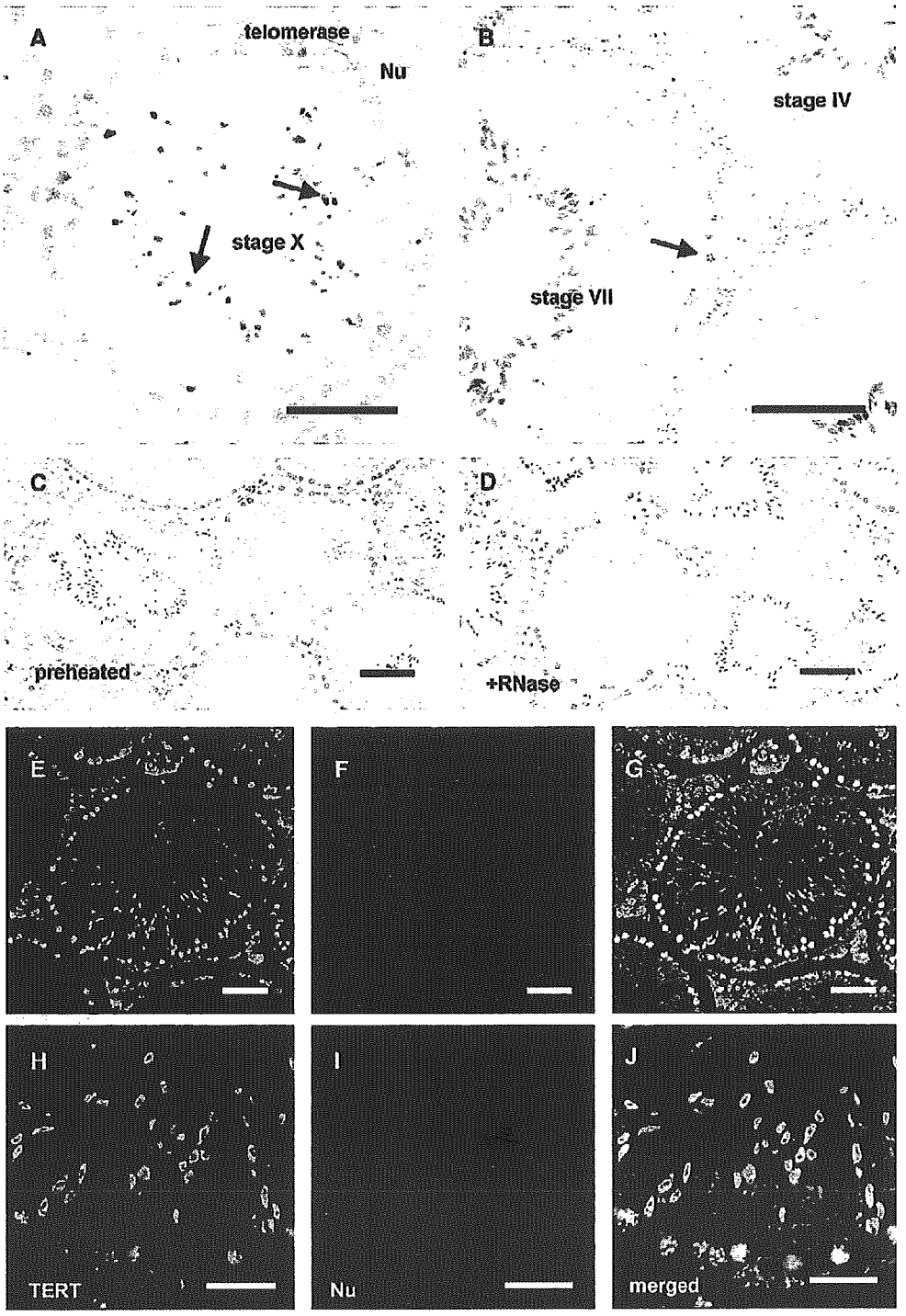

Fig. 3. Telomerase activity and telomerase catalytic subunit (TERT) expression in mature mouse testes. (A–D) In situ TRAP analysis of testis sections from a mature mouse. Brown signals (arrows) represent telomerase activity. Nuclei were stained with hematoxylin. (A) Seminiferous tubule at stage X. Strong signals were detected in step 10 elongating spermatids. (B) Seminiferous tubule at stages IV and VII. Signals were detected in intermediate spermatogonia (stage IV) and preleptotene spermatocytes (stage VII). Few signals were detected in pachytene spermatocytes, round spermatids, or elongated spermatids. (C, D) Negative control experiments for in situ TRAP. No signals were detected when samples were either preheated at 85°C (C) or pretreated with RNase (D). (E–J) TERT immunohistochemistry of stage X seminiferous tubules (E–G) and seminiferous epithelia (H–J). (E, H) Green signals represent TERT expression. (F, I) Red signals represent propidium iodide nuclear staining. (G, J) Merged image. (A–G) Scale bar = 50 μm. (H–J) Scale bar = 25 μm.

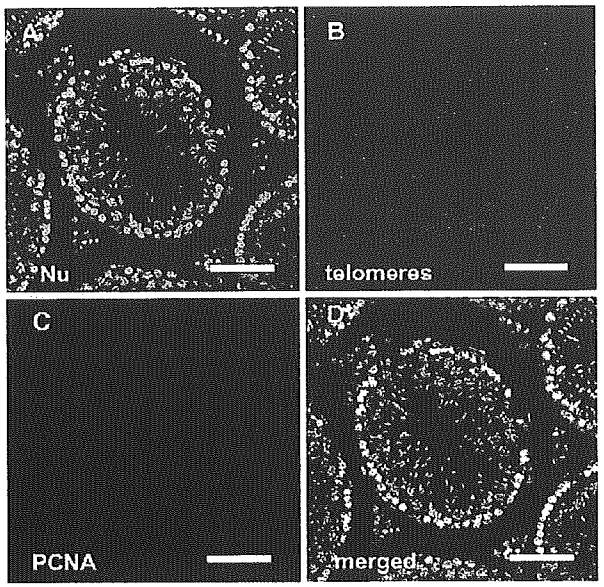

Fig. 4. (A–D) FISH analysis and immunohistochemistry of stage X seminiferous tubules. (A) Green signals represent SYTE-Green-stained nuclei. (B) Red signals represent telomeres. (C) Blue signals represent proliferating cells stained with anti-PCNA monoclonal antibody. (D) Merged image. (A–D, F–I) Scale bar = 50 μm.

epithelium, cell types in which telomere extension occurs (Figs. 3E–J). These observations also agree well with our FISH (Fig. 1O) and in situ TRAP assay (Fig. 3A) results. Interestingly, not all elongating spermatids were TERT immunoreactive, suggesting that TERT expression occurs in a mosaic pattern in elongating spermatids, and that an alternative telomere extension pathway is at work in some elongating spermatids lacking TERT immunoreactivity.

Another important aspect of telomere extension in spermatids is that telomeric DNA synthesis is not coupled with cell replication. By contrast, telomeric DNA synthesis in mitotic cells is coupled with cell replication since telomere extension in these cells occurs during the S-phase (Masutomi et al., 2003; Zhu et al., 1996). By the time spermatids are formed, it is well established that chromosomal replication and cell division have already finished. In fact, we detected proliferating cell nuclear antigen (PCNA), an S-phase marker, only in cells undergoing DNA replication, such as in spermatogonia and preleptotene spermatocytes, and never in elongating spermatids (Figs. 4A–D). Thus, the telomere extension activity in haploid cells can be different from the conventional telomerase activity observed in somatic cells during proliferation (Fig. 5).

Analysis of testes from telomerase-deficient mice

Telomerase mutant mice are capable of reproducing during the first through fifth generations; however, after the sixth generation, these mice become infertile, losing the capability of reproducing (Blasco et al., 1997; Lee et al., 1998). Thus, at some step during germ cell production in these animals, a complementary mechanism for extending telomeres must exist. We examined telomeric rearrangement during spermatogenesis in second generation (G2) telomerase (RNA component)-null ($Terc^{-/-}$) mice (Blasco et al., 1997; Lee et al., 1998). Telomere length in elongated spermatids from these mice varied such that some had long telomeres, while others had short telomeres (Figs. 6A–H). This indicates that telomere extension in elongating spermatids is partially impaired in G2 $Terc^{-/-}$ mice (Fig. 6F). Histochemical analysis with soybean agglutinin (SBA), a differential marker for elongated spermatids (Figs. 6I–K; Martinez-Menarguez et al., 1999), revealed fewer intact sperm in $Terc^{-/-}$ mice (Figs. 6M, P) compared to that in $Terc^{+/-}$ mice (Fig. 6L). This was apparently not due to a

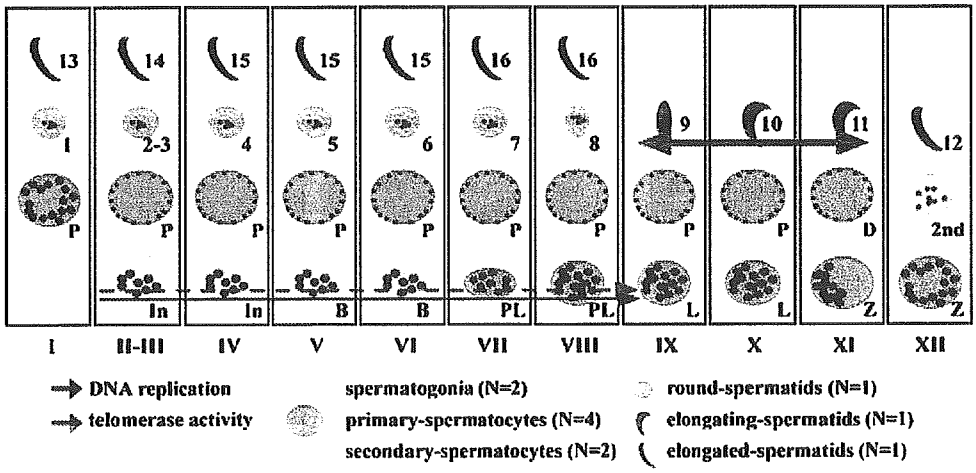

Fig. 5. Schematic diagram of telomere dynamics during spermatogenesis. Large circles (khaki, green, blue, and azure) and crescents (navy blue) represent nuclei of spermatogenic cells. Intermediate spermatogonia (In), type B spermatogonia (B), preleptotene spermatocytes (PL), leptotene spermatocytes (L), zygotene spermatocytes (Z), pachytene spermatocytes (P), diplotene spermatocytes (D), secondary spermatocytes (2nd), round spermatids (steps 1–8), elongating spermatids (steps 9–12), and elongated spermatids (steps 13–16). Telomeres are indicated as red dots within the nuclei. Blue and pink arrows indicate the presence of telomere extension activity and DNA replication activity, respectively.

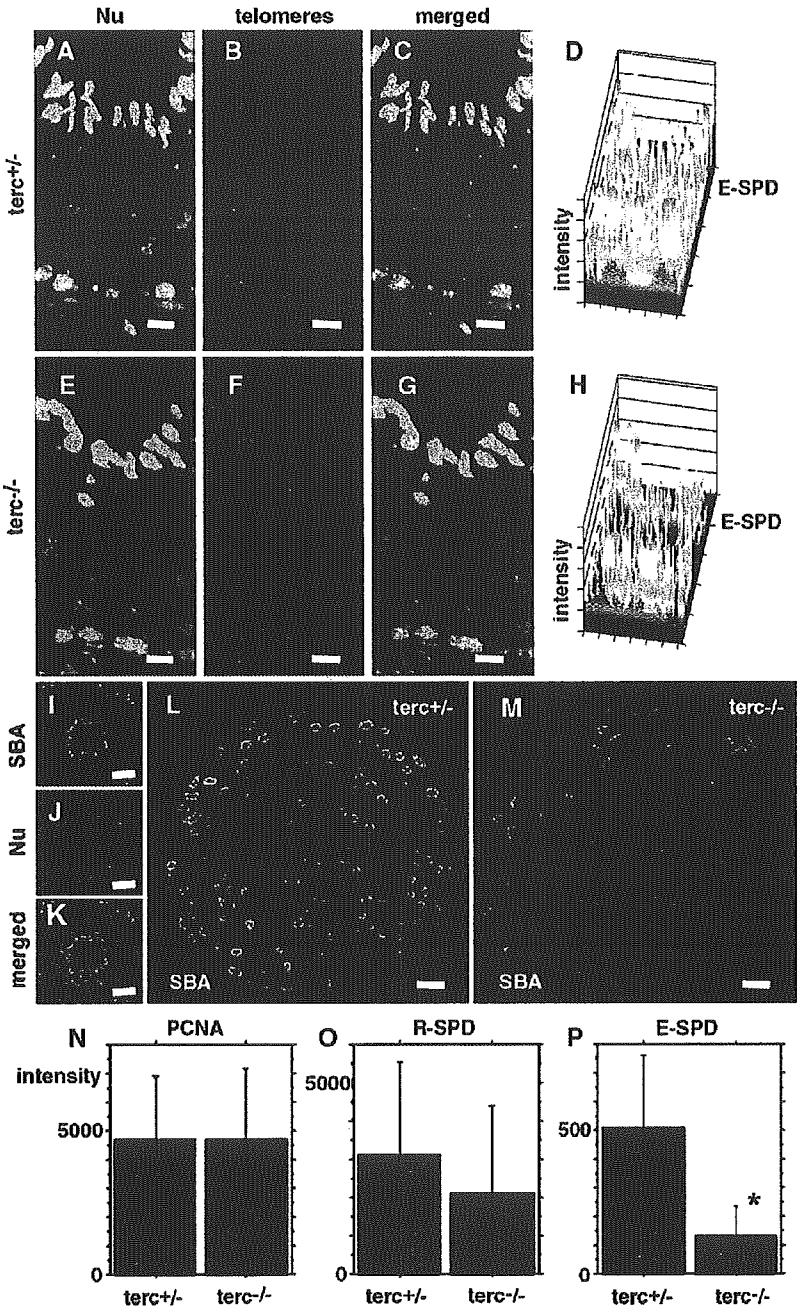

Fig. 6. FISH analysis and lectin histochemistry of testis sections from a telomerase null mouse. (A–D) FISH analysis of stage VIII seminiferous epithelia from a *Terc*$^{+/-}$ mouse. (E–H) FISH analysis of stage VIII seminiferous epithelia from a G2 *Terc*$^{-/-}$ mouse. (A, E) Green signals represent SYTE-Green-stained nuclei. (B, F) Red signals represent telomeres. (C, G) Merged images. (D, H) Visualization of telomeric signal intensity. Red indicates strong signals, yellow moderate signals, and green weak signals. (I–M) SBA lectin-stained seminiferous tubules from a *Terc*$^{+/-}$ mouse (I–L) and a G2 *Terc*$^{-/-}$ mouse (M). (I–K) Stage I seminiferous tubule. (L, M) Cross-sections of whole mouse testis. (I, L, M) Green signals represent SBA reactivities. (J) Red signals represent propidium iodide nuclear staining. (K) Merged images. (N) Quantitative analysis of PCNA immunoreactivity in the testes of *Terc*$^{+/-}$ and G2 *Terc*$^{-/-}$ mice (PCNA). (O) Quantitative analysis of SBA reactivity in the round spermatids of *Terc*$^{+/-}$ and G2 *Terc*$^{-/-}$ mice (R-SPD). (P) Quantitative analysis of SBA reactivity in elongating and elongated spermatids of *Terc*$^{+/-}$ and G2 *Terc*$^{-/-}$ mice (E-SPD). *$P < 0.05$; (A–H) Scale bar = 10 μm; (I–K) Scale bar = 50 μm; (L, M) Scale bar = 500 μm.

reduction in proliferative spermatogenic cells, since the number of PCNA-immunoreactive cells was basically the same in *Terc*$^{+/-}$ and *Terc*$^{-/-}$ mice (Fig. 6N). Moreover, there was no significant difference in the number of round spermatids among these mice (Fig. 6O), suggesting that the maturation step between the round spermatid and elongated spermatid stages was partially impaired in *Terc*$^{-/-}$ mice. Although *Terc*$^{-/-}$ mice had fewer intact sperm containing

extended telomeres than their wild-type or $Terc^{+/-}$ littermates, they still produced elongating spermatids that had the capacity to extend telomeres successfully, thus forming intact sperm and allowing the animal to maintain fertility. This suggests that alternative, non-*Terc*, telomere extension activity (Bryan et al., 1997; Dunham et al., 2000; Niida et al., 2000; Reddel, 2003) is at work in these mice and that this alternative system is capable of partially complementing the telomerase defect in $Terc^{-/-}$ mice.

Discussion

Many genes at work in biological processes are regulated in a cell-specific manner. Recently, it has been proposed that the three-dimensional structure of chromosomes within the nucleus is important for cellular activities (Kosak and Groudine, 2004). Telomeres can be one obvious positional cue responsible for the nuclear arrangement of chromosomes. In the present study, we used improved Q-FISH and in situ TRAP assays to investigate telomere dynamics during spermatogenesis. The movement of telomeres we observed agreed well with those described previously (Meyer-Ficca et al., 1998; Pfeifer et al., 2001; Scherthan et al., 1996; Zalenskaya and Zalensky, 2002, 2004). Application of this improved Q-FISH technique on testis tissue sections allowed us to observe the full spectrum of telomere dynamics in developing spermatogenic cells, starting from the beginning of spermatogenesis (stage I) to the end of spermatogenesis (stage XII).

During different steps of spermatogenesis, fluctuations were observed in telomere signal intensity, reflecting changes in telomere length. We also observed some novel events: telomere shortening occurs in pachytene spermatocytes and subsequent telomere amplification occurs in elongating spermatids. Our data from TRAP assays and TERT immunohistochemistry were in good agreement and consistently supported these findings. In the present study using mice, telomerase activity disappeared during the pachytene spermatocyte phase, whereas in rat (Achi et al., 2000), telomerase activity persisted throughout spermatogenesis. This apparent discrepancy can be explained by species or methodological differences. Although the significance and mechanisms of this fluctuation remain elusive, the telomere movement and telomere length may correlate each other. Telomere shortening during pachytene spermatocyte phase can be important in subsequent moving telomeres away from the nuclear periphery, since longer telomeres probably make the movement more difficult.

Telomerase activity (as measured with TRAP) and TERT immunoreactivity simultaneously increased in elongating spermatids, which is in good agreement with the increased intensity of telomere signals. As a consequence of this increased telomerase activity, sperm have extremely long telomeres. It is possible that germ cells require long telomeres to prepare for several rounds of successive replication after fertilization despite the absence of new transcription products during replication. Thus, we propose that extra-long telomeres in sperm are important for determining the individual life span of genetic descendants, although there is no clear description on female germ cells yet. This hypothesis is supported by the finding that sperm from G2 and G3 $Terc^{-/-}$ mice exhibit lower ratios of fertilization and higher frequencies of early developmental failure in comparison with sperm from $Terc^{+/+}$ mice (Liu et al., 2002), even though active spermatogenesis can be detected in $Terc^{-/-}$ mice up to the fourth generation (Lee et al., 1998). The observation that telomere extension activity is preserved during germ cell production, even in the absence of the telomerase complex, strongly suggests the existence of alternative telomere synthetic pathway(s) (Bryan et al., 1997; Dunham et al., 2000; Niida et al., 2000; Reddel, 2003) and the importance of telomere extension for proper sperm formation. Together with our data on the number of properly generated sperm, these findings indicate that impairment of telomere synthesis may cause multiple defects, starting in spermiogenesis to early development.

TERT immunoreactivities revealed that an authentic telomerase complex is not present in all elongating spermatids, even though telomere extension seems to have taken place in all the elongating spermatids by FISH analyses we examined. This discrepancy further indicates that alternative telomere extension activity is at work during spermiogenesis, even in wild-type animals. It has been suggested that one alternative way telomeres lengthen is by recombination and intertelomeric copying of DNA (Dunham et al., 2000). In this hypothesis, the nuclear gathering of telomeres that occurs in elongating spermatids is required for extension, since the close positioning of telomeres greatly raises the chance of intertelomeric recombination. This process requires DNA-directed DNA polymerases. Elongating spermatids possess several DNA polymerases, probably for repair and recombination events (data not shown) (Garcia-Diaz et al., 2000; Ogi et al., 2001; Plug et al., 1997).

In the present report, we described two powerful techniques to analyze the nuclear organization of telomeres, to compare the approximate lengths of telomeric repeats, and to map the position of telomeres within the nucleus. First, the improved FISH technique carried out on histological sections permits the correlation of cell stage and corresponding chromosomal state during development. In yeast, it is well known that the relative position of telomeres within the nucleus impacts the transcription state of genetic loci (Andrulis et al., 1998). However, in mammals, the role of telomere dynamics and position is less understood since contradictory observations have been reported (Ferguson and Ward, 1992; Luderus et al., 1996). Although some stages of telomere dynamics have already been partially described (Meyer-Ficca et al., 1998; Pfeifer et al., 2001; Scherthan et al., 1996; Zalenskaya and Zalensky, 2002,

2004), by implementing these improved techniques, we were able to determine that changes in telomere position and length occur in a dynamic continuum.

The in situ TRAP assay permits detection of telomere synthesis activity at the resolution of a single cell within histological sections. Application of the in situ TRAP assay is not restricted to the study of chromosomal organization. Because it is well known that most immortal cells exhibit telomerase activity and show positive TRAP reactions, we expect that the in situ TRAP assay can be a very powerful tool to rapidly identify and localize tumors and cancers to specific cell types. Valuable information on tumor cell morphology, as well as on telomerase activities in individual cells, can be simultaneously collected. Moreover, the in situ TRAP technique is highly sensitive. In our experiments, we were able to detect telomerase activity in cells located in interstitial areas of the mouse testis; such low-level activity would have been missed with conventional TRAP assay techniques. In addition, the in situ TRAP assay will contribute greatly to verifying the validity of various medical treatments as well as to the development of customized cancer drugs to treat individual cases of cancer.

Acknowledgments

We thank R.A. DePinho for providing the *Terc* knockout mice and the critical reading of the manuscript. We are grateful to S. Gasser for the critical reading of the manuscript and to the members of the Kondo Laboratory for sharing reagents. T.K. also would like to thank D. Duboule and M. Muramatsu for continuous encouragement, and the late G. Matsumoto for help in establishing the laboratory. T.K. is supported by a grant from the Human Frontier Scientific Program Organization (HFSPO) and Grant-in-Aid for Scientific Research on Priority Areas from The Ministry of Education, Culture, Sports, and Technology (MEXT) of Japan. K.T. is also funded by Grant-in-Aid for Scientific Research on Priority Areas from MEXT. Correspondence and requests for materials should be addressed to T.K. (TKondo@brain.riken.go.jp).

References

Achi, M.V., Ravindranath, N., Dym, M., 2000. Telomere length in male germ cells is inversely correlated with telomerase activity. Biol. Reprod. 63, 591–598.

Andrulis, E.D., Neiman, A.M., Zappulla, D.C., Sternglanz, R., 1998. Perinuclear localization of chromatin facilitates transcriptional silencing. Nature 394, 592–595.

Biggiogera, M., Muller, S., Courtens, J.L., Fakan, S., Romanini, M.G., 1992. Immunoelectron microscopical distribution of histones H2B and H3 and protamines in the course of mouse spermatogenesis. Microsc. Res. Tech. 20, 259–267.

Blasco, M.A., Funk, W., Villeponteau, B., Greider, C.W., 1995. Functional characterization and developmental regulation of mouse telomerase RNA. Science 269, 1267–1270.

Blasco, M.A., Lee, H.W., Hande, M.P., Samper, E., Lansdorp, P.M., DePinho, R.A., Greider, C.W., 1997. Telomere shortening and tumor formation by mouse cells lacking telomerase RNA. Cell 91, 25–34.

Bryan, T.M., Englezou, A., Dalla-Pozza, L., Dunham, M.A., Reddel, R.R., 1997. Evidence for an alternative mechanism for maintaining telomere length in human tumors and tumor-derived cell lines. Nat. Med. 3, 1271–1274.

Cremer, T., Cremer, C., 2001. Chromosome territories, nuclear architecture and gene regulation in mammalian cells. Nat. Rev., Genet. 2, 292–301.

de Lange, T., 2002. Protection of mammalian telomeres. Oncogene 21, 532–540.

Dietzel, S., Belmont, A.S., 2001. Reproducible but dynamic positioning of DNA in chromosomes during mitosis. Nat. Cell Biol. 3, 767–770.

Ducray, C., Pommier, J.P., Martins, L., Boussin, F.D., Sabatier, L., 1999. Telomere dynamics, end-to-end fusions and telomerase activation during the human fibroblast immortalization process. Oncogene 18, 4211–4223.

Dunham, M.A., Neumann, A.A., Fasching, C.L., Reddel, R.R., 2000. Telomere recombination in human cells. Nat. Genet. 26, 447–450.

Felder, D.M., Hackett, J.M., Greider, C.W., 2003. Telomere dysfunction and the initiation of genome instability. Nat. Rev., Cancer 3, 623–627.

Ferguson, M., Ward, D.C., 1992. Cell cycle dependent chromosomal movement in pre-mitotic human T-lymphocyte nuclei. Chromosoma 101, 557–565.

Franco, S., Alsheimer, M., Herrera, E., Benavente, R., Blasco, M.A., 2002. Mammalian meiotic telomeres: composition and ultrastructure in telomerase-deficient mice. Eur. J. Cell Biol. 81, 335–340.

Garcia-Diaz, M., Dominguez, O., Lopez-Fernandez, L.A., de Lera, L.T., Saniger, M.L., Ruiz, J.F., Parraga, M., Garcia-Ortiz, M.J., Kirchhoff, T., del Mazo, J., Bernad, A., Blanco, L., 2000. DNA polymerase lambda (Pol lambda), a novel eukaryotic DNA polymerase with a potential role in meiosis. J. Mol. Biol. 301, 851–867.

Gasser, S.M., 2002. Visualizing chromatin dynamics in interphase nuclei. Science 296, 1412–1416.

Gerlich, D., Beaudouin, J., Kalbfuss, B., Daigle, N., Eils, R., Ellenberg, J., 2003. Global chromosome positions are transmitted through mitosis in mammalian cells. Cell 112, 751–764.

Gonzalez-Suarez, E., Samper, E., Flores, J.M., Blasco, M.A., 2000. Telomerase-deficient mice with short telomeres are resistant to skin tumorigenesis. Nat. Genet. 26, 114–117.

Gotta, M., Laroche, T., Formenton, A., Maillet, L., Scherthan, H., Gasser, S.M., 1996. The clustering of telomeres and colocalization with Rap1, Sir3, and Sir4 proteins in wild-type *Saccharomyces cerevisiae*. J. Cell Biol. 134, 1349–1363.

Greenberg, R.A., Allsopp, R.C., Chin, L., Morin, G.B., DePinho, R.A., 1998. Expression of mouse telomerase reverse transcriptase during development, differentiation and proliferation. Oncogene 16, 1723–1730.

Greider, C.W., 1996. Telomere length regulation. Annu. Rev. Biochem. 65, 337–365.

Greider, C.W., Blackburn, E.H., 1996. Telomeres, telomerase and cancer. Sci. Am. 274, 92–97.

Grosveld, F., 1999. Activation by locus control regions? Curr. Opin. Genet. Dev. 9, 152–157.

Guarente, L., 1999. Diverse and dynamic functions of Sir silencing complex. Nat. Genet. 23, 281–285.

Hastie, N.D., Dempster, M., Dunlop, M.G., Thompson, A.M., Green, D.K., Allshire, R.C., 1990. Telomere reduction in human colorectal carcinoma and with ageing. Nature 346, 866–868.

Henderson, S., Allsopp, R., Spector, D., Wang, S.S., Harley, C., 1996. In situ analysis of changes in telomere size during replicative aging and cell transformation. J. Cell Biol. 134, 1–12.

Hiyama, E., Hiyama, K., 2002. Clinical utility of telomerase in cancer. Oncogene 21, 643–649.

Kim, N.W., Piatyszek, M.A., Prowse, K.R., Harley, C.B., West, M.D., Ho, P.L., Coviello, G.M., Wright, W.E., Weinrich, S.L., Shay, J.W., 1994.

Specific association of human telomerase activity with immortal cells and cancer. Science 266, 2011–2015.
Kosak, S.T., Groudine, M., 2004. Form follows function: the genomic organization of cellular differentiation. Genes Dev. 18, 1371–1384.
Leblomd, C.P., Clermont, Y., 1952. Spermatogenesis of rat, mouse, hamster, and guinea pig as revealed by the "periodic acid-fuchsin sulfurous acid" technique. Am. J. Anat. 90, 167–215.
Lee, H.W., Blasco, M.A., Gottlieb, G.J., Homer II, J.W., Greider, C.W., DePinho, R.A., 1998. Essential role of mouse telomerase in highly proliferative organs. Nature 392, 569–574.
Liu, L., Blasco, M.A., Trimarchi, J., Keefe, D., 2002. An essential role for functional telomeres in mouse germ cells during fertilization and early development. Dev. Biol. 249, 74–84.
Luderus, M.E., van Steensel, B., Chong, L., Sibon, O.C., Cremers, F.F., de Lange, T., 1996. Structure, subnuclear distribution, and nuclear matrix association of the mammalian telomeric complex. J. Cell Biol. 135, 867–881.
Martinez-Menarguez, J.A., Abascal, I., Aviles, M., Castells, M.T., Ballesta, J., 1999. Cytochemical and Western blot analysis of the subcompartmentalization of the acrosome in rodents using soybean lectin. Histochem. J. 31, 19–37.
Masutomi, K., Yu, E.Y., Khurts, S., Ben-Porath, I., Currier, J.L., Metz, G.B., Brooks, M.W., Kaneko, S., Murakami, S., DeCaprio, J.A., Weinberg, R.A., Stewart, S.A., Hahn, W.C., 2003. Telomerase maintains telomere structure in normal human cells. Cell 114, 241–253.
Meeker, A.K., Gage, W.R., Hicks, J.L., Simon, I., Coffman, J.R., Platz, E.A., March, G.E., De Marzo, A.M., 2002. Telomere length assessment in human archival tissues. Am. J. Pathol. 160, 1259–1268.
Meyer-Ficca, M., Muller-Navia, J., Scherthan, H., 1998. Clustering of pericentromeres initiated in step 9 of spermiogenesis of the rat (*Rattus norvegicus*) and contributes to a well defined genome architecture in the sperm nucleus. J. Cell Sci. 111, 1363–1370.
Molenaar, C., Wiesmeijer, K., Verwoerd, N.P., Khazen, S., Eils, R., Tanke, H.J., Dirks, R.W., 2003. Visualizing telomere dynamics in living mammalian cells using PNA probes. EMBO J. 22, 6631–6641.
Nakamura, T.M., Morin, G.B., Chapman, K.B., Weinrich, S.L., Andrews, W.H., Lingner, J., Harley, C.B., Cech, T.R., 1997. Telomerase catalytic subunit homologs from fission yeast and human. Science 277, 955–959.
Niida, H., Shinkai, Y., Hande, M.P., Matsumoto, T., Takehara, S., Tachibana, M., Oshimura, M., Lansdorp, P.M., Furuichi, Y., 2000. Telomere maintenance in telomerase-deficient mouse embryonic stem cells: characterization of an amplified telomeric DNA. Mol. Cell. Biol. 20, 4115–4127.
Ogi, T., Mimura, J., Hikida, M., Fujimoto, H., Fujii-Kuriyama, Y., Ohmori, H., 2001. Expression of human and mouse genes encoding polkappa: testis-specific developmental regulation and AhR-dependent inducible transcription. Genes Cells 6, 943–953.
Pfeifer, C., Thomsen, P.D., Scherthan, H., 2001. Centromere and telomere redistribution precedes homologue pairing and terminal synapsis initiation during prophase I of cattle spermatogenesis. Cytogenet. Cell Genet. 93, 304–314.
Pfeifer, C., Scherthan, H., Thomsen, P.D., 2003. Sex-specific telomere redistribution and synapsis initiation in cattle oogenesis. Dev. Biol. 255, 206–215.
Plug, A.W., Clairmont, C.A., Sapi, E., Ashley, T., Sweasy, J.B., 1997. Evidence for a role for DNA polymerase beta in mammalian meiosis. Proc. Natl. Acad. Sci. U. S. A. 94, 1327–1331.
Prowse, K.R., Greider, C.W., 1995. Developmental and tissue-specific regulation of mouse telomerase and telomere length. Proc. Natl. Acad. Sci. U. S. A. 92, 4818–4822.
Reddel, R.R., 2003. Alternative lengthening of telomeres, telomerase, and cancer. Cancer Lett. 194, 155–162.
Russell, L.D., Ettlin, R.A., Sinha Hikim, A.P., Clegg, E.D., 1990. Histological and histopathological evaluation of the testis. Cache River Press.
Scherthan, H., 2001. A bouquet makes ends meet. Nat. Rev., Mol. Cell Biol. 2, 621–627.
Scherthan, H., Weich, S., Schwegler, H., Heyting, C., Harle, M., Cremer, T., 1996. Centromere and telomere movements during early meiotic prophase of mouse and man are associated with the onset of chromosome pairing. J. Cell Biol. 134, 1109–1125.
Wong, J.M., Collins, K., 2003. Telomere maintenance and disease. Lancet 362, 983–988.
Zalenskaya, I.A., Zalensky, A.O., 2002. Telomeres in mammalian male germline cells. Int. Rev. Cytol. 218, 37–67.
Zalenskaya, I.A., Zalensky, A.O., 2004. Non-random positioning of chromosomes in human sperm nuclei. Chromosome Res. 12, 163–173.
Zhu, X., Kumar, R., Mandal, M., Sharma, N., Sharma, H.W., Dhingra, U., Sokoloski, J.A., Hsiao, R., Narayanan, R., 1996. Cell cycle-dependent modulation of telomerase activity in tumor cells. Proc. Natl. Acad. Sci. U. S. A. 93, 6091–6095.

Human Reproduction Vol.20, No.9 pp. 2376–2382, 2005 doi:10.1093/humrep/dei096
Advance Access publication May 26, 2005

Germline niche transplantation restores fertility in infertile mice

M.Kanatsu-Shinohara[1,2], H.Miki[3], K.Inoue[3], N.Ogonuki[3], S.Toyokuni[4], A.Ogura[3] and T.Shinohara[2,5]

[1]Horizontal Medical Research Organization and [4]Department of Pathology and Biology of Diseases, Graduate School of Medicine, Kyoto University, Kyoto 606-8501, [2]Department of Molecular Genetics, Graduate School of Medicine, Kyoto University, Kyoto 606-8507 and [3]The Institute of Physical and Chemical Research (RIKEN), Bioresource Center, Ibaraki 305-0074, Japan

[5]To whom correspondence should be addressed. E-mail: tshinoha@virus.kyoto-u.ac.jp

BACKGROUND: Stem cells interact closely with their microenvironment or niche, and abnormalities in niche compromise the self-renewing tissue. In testis, for example, Sertoli cells interact with germ cells, and defects in Sertoli cells compromises spermatogenesis, leading to male infertility. However, it has not been possible to restore spermatogenesis from endogenous stem cells in infertile testis with environmental defects METHODS AND RESULTS: When healthy Sertoli cells from infertile white spotting (W) mouse were transplanted into the seminiferous tubules of infertile Steel (Sl) mouse testis that had defective Sertoli cells, spermatogenesis occurred from Sl stem cells in the recipient testis. On average, 1.1% of the recipient tubules showed spermatogenesis. Furthermore, in a microinsemination experiment with germ cells that developed in the testis, we obtained four normal offspring from 114 successfully injected oocytes. CONCLUSIONS: This study demonstrates that defects in male germline microenvironment can be corrected by Sertoli cell transplantation. Although further improvements are required to enhance the low efficiency of spermatogenesis, the ability to correct environmental defect by niche transplantation has important implications in developing new strategies for treating incurable disorders in self-renewing tissues.

Key words: infertility/niche/Sertoli cells/spermatogenesis/transplantation

Introduction

Spermatogenesis occurs within the seminiferous tubules, which are composed of germ cells, Sertoli cells, and peritubular cells. Although Sertoli cells comprise only 3% of the total testis cell population (Bellvé, 1993), they are the only somatic cells that interact directly with germ cells, thereby constituting the primary cellular component of germline niche (Spradling *et al.*, 2001). Because they provide structural and nutritional support for spermatogenesis, the disruption of this crucial relationship results in male infertility. For example, the lack of expression of membrane-bound Steel factor on Sertoli cells in infertile Steel (Sl) mutant mice prevents the differentiation of spermatogonia that express c-kit receptor, resulting in azoospermia (Flanagan *et al.*, 1991). In contrast, the germ cells in infertile white spotting (W) mice have mutations in the c-kit receptor, causing a similar condition (Geissler *et al.*, 1988). However, when spermatogonial stem cells from Sl mice were transplanted into the testes of W mice that had normal Sertoli cells, complete spermatogenesis occurred and offspring were produced from the transplanted Sl stem cells (Ogawa *et al.*, 2000). Thus, the interaction between Sertoli cells and germ cells is critical for spermatogenesis, and the restoration of physiological interactions between germ cells and Sertoli cells by germ cell transplantation allows the complete differentiation of spermatogonial stem cells. Interestingly, a similar relationship exists in other self-renewing tissues; defects in haematopoiesis and melanogenesis in Sl and W mutants can be rescued by the transplantation of cell populations from Sl mice into W recipient mice (McCulloch *et al.*, 1965; Mayer and Green, 1968). However, the reciprocal transplantation of cells from W mice or wild-type mice into Sl recipients has failed to restore normal function (McCulloch *et al.*, 1965; Mayer and Green, 1968), and it has not been possible to replace the defective microenvironment to rescue stem cells *in situ*.

Recently, we have shown the feasibility of transplanting Sertoli cells (Shinohara *et al.*, 2003). Sertoli cells isolated from the donor testis could colonize the seminiferous tubules of the infertile recipient testis following microinjection. The colonizing activity was enhanced significantly when the recipient Sertoli cells were eliminated by cadmium treatment or when the donor Sertoli cells were prepared from immature testes in which the Sertoli cells were mitotically active. The dissociated donor cells reaggregated after transplantation to

form a seminiferous tubule-like structure ('minitubule'), and spermatogenesis was detected in the recipient testis. Although these studies demonstrated spermatogenesis in the tubule-like aggregates, it has not been possible to induce the recovery of spermatogenesis from endogenous stem cells. This was an important goal, since it is necessary to use endogenous germ cells in the host to rescue infertility in clinical situations. Our present results provide evidence that a similar process of reorganization occurred *in vivo* with heterologous testis cells in the seminiferous tubules of the recipient mice.

Materials and methods

Animals

Both WBB6F1-Sl/Sl^{d} and WBB6F1-W/W^{v} mice were purchased from Japan SLC (Shizuoka, Japan). Single cell suspensions were prepared from the testes of neonatal (0–2 day old) W and mature (4–6 week old) Sl mice using a two-step enzymatic digestion as previously described (Ogawa *et al.*, 1997). In brief, the testis cells were digested with 1 mg/ml collagenase (type IV; Sigma, St Louis, MO, USA) for 15 min, followed by digestion with 0.25% trypsin/1 mmol/l EDTA (both from Invitrogen, Carlsbad, CA, USA) for 10 min. The cell suspensions were filtered through nylon mesh with a 30 μm pore size before transplantation.

For transplantation of the prepared testis cells, ~3 μl of the donor cell suspensions were injected into the seminiferous tubules of the testes of each 4–6 week old Sl recipient mouse through the efferent duct (Ogawa *et al.*, 1997). The cells were injected at a concentration of 8.3×10^7 cells/ml. In some experiments, 4 weeks after the transplantation of cells from W mice, the recipient Sl mice were given an additional transplantation of 3×10^5 testis cells from another Sl mouse. The injections filled 75–85% of the tubules in all recipient testes. The estimated concentration of Sertoli cells was ~3.7×10^7 cells/ml. In both cases, ~2.5×10^5 testis cells from W mice (approximately equivalent to one-half W testis) were microinjected into the testes of each Sl recipient.

A total of four experiments was performed. Eighteen Sl testes received only W testis cells, and six Sl testes received both W and additional Sl testis cells by injection into the seminiferous tubules. All of the animal experimentation protocols were approved by the Institutional Animal Care and Use Committee of Kyoto University.

Analysis

Two to 3 months after the transplantation, the mice were killed and the testes were fixed with 10% neutral-buffered formalin and processed for paraffin sectioning. Two histological sections were made from each recipient testis with an interval of 12 μm between sections. All sections were stained with haematoxylin and eosin. Each slide was viewed at a magnification of ×400 to determine the extent of spermatogenesis. The number of tubule cross-sections with or without spermatogenesis, defined as the presence of multiple layers of spermatogenic cells in the entire circumference of the seminiferous tubule, was recorded for one histological section from each testis.

Microinsemination

Two recipients that had been transplanted with testis cells from W mice were killed at 6 months after transplantation. The testes were mechanically dissociated, and live spermatogenic cells were recovered by repeated pipetting of the seminiferous tubules. Round spermatids, as identified by a small round nucleus with a uniquely shaped chromatin mass, were microinjected into oocytes derived from C57BL/6 × DBA/2 F1 mice. About 80% of oocytes survived the injection procedure irrespective of the day of experiment. Microinsemination was performed as previously described using round spermatids (Kimura and Yanagimachi, 1995). Embryos that reached the 2-cell stage after 24 h in culture were transferred to the oviducts of day 0.5 (the day following sterile mating) pseudopregnant (ICR) females. Live fetuses retrieved on day 19.5 were raised by lactating foster ICR mothers.

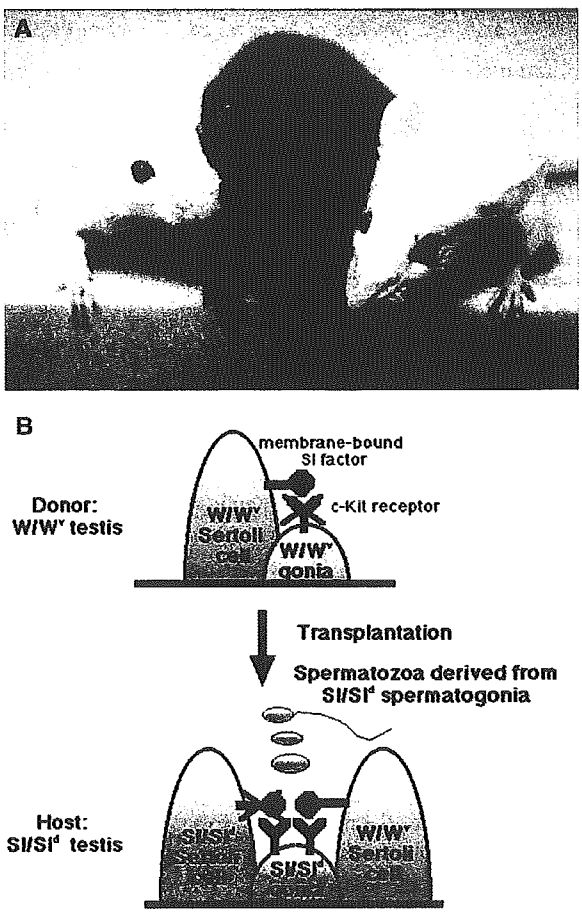

Figure 1. Overview of Sertoli cell transplantation. (**A**) Appearance of infertile white spotting (W) and infertile Steel (Sl) mouse mutants. W (left) and Sl (right) have defects in hematopoiesis, melanogenesis and gametogenesis attributable to defects in the *c-kit* and *Sl* genes respectively. Owing to defective melanogenesis, the W and Sl mutants have a white coat colour and are indistinguishable from each other on the basis of appearance, whereas the wild-type C57BL6 mouse (middle) has a black coat colour. (**B**) A schematic outline of Sertoli cell transplantation. The germ cells in W mice have a defect in the c-kit receptor and cannot transduce the signal from the Sl factor. On the other hand, the Sertoli cells in Sl mice do not express the membrane-bound Sl factor, and cannot induce normal germ cell differentiation. The transplantation of W Sertoli cells into the Sl testis triggers spermatogenesis from the endogenous Sl germ cells, resulting in the production of differentiated germ cells carrying defective Sl genes.